Hinode: A Decade of Success in Capturing Solar Activity

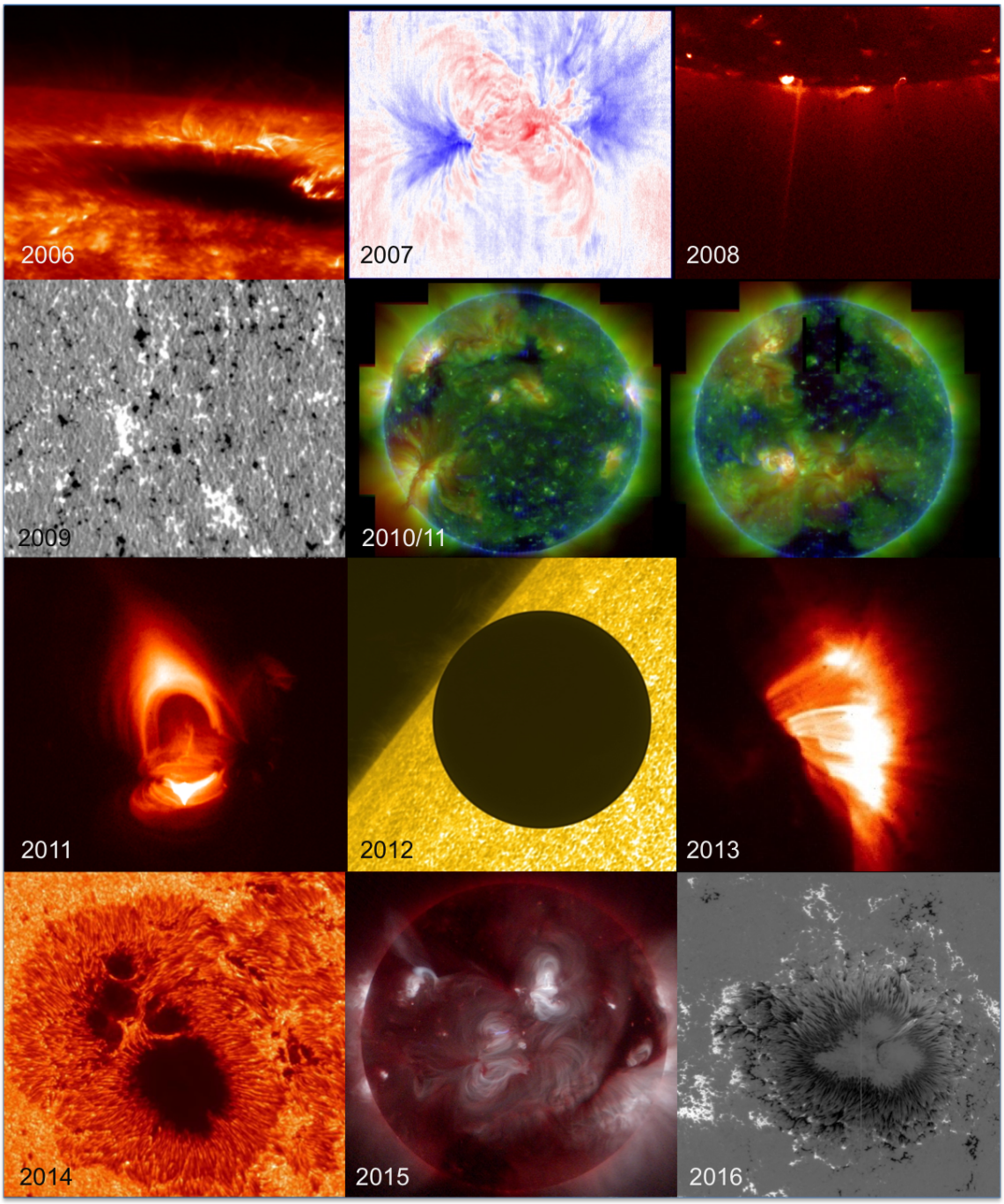

A proposal to the Senior Review of Heliophysics Operating Missions
February 2017

Prepared by:
S. Savage, US Project Scientist, NASA MSFC
S. Elrod, Project Manager, NASA MSFC
E. DeLuca, XRT NASA Principal Investigator, SAO
G. Doschek → H. Warren, EIS Principal Investigator, NRL
T. Tarbell, SOT NASA Principal Investigator, LMSAL
...and the entire Hinode Project Team

TABLE OF CONTENTS

Hinode: A Decade of Success in Capturing Solar Activity

SCIENCE and SCIENCE IMPLEMENTATION

1 INTRODUCTION

As the present solar cycle passes into its minimum phase, the *Hinode* mission marks its tenth year of investigating solar activity. *Hinode*'s decade of successful observations have provided us with immeasurable insight into the solar processes that invoke space weather and thereby affect the interplanetary environment in which we reside. The mission's complementary suite of instruments allows us to probe transient, high energy events alongside long-term, cycle-dependent phenomena from magnetic fields at the Sun's surface out to highly thermalized coronal plasma enveloping active regions (ARs). These rich data sets have already changed the face of solar physics and will continue to provoke exciting research as new observational paradigms are pursued.

Hinode was launched as part of the Science Mission Directorate's (SMD) Solar Terrestrial Probes Program in 2006. It is a sophisticated spacecraft equipped with a Solar Optical Telescope (SOT), an Extreme-ultraviolet Imaging Spectrometer (EIS), and an X-Ray Telescope (XRT) (see § 4). With high resolution and sensitivity, *Hinode* serves as a microscope for the Sun, providing us with unique capabilities for observing magnetic fields near the smallest scales achievable, while also rendering full-Sun coronal context in the highest thermal regimes.

The 2014 NASA SMD strategic goals objective to "Understand the Sun and its interactions with the Earth and the solar system, including space weather" forms the basis of three underlying Heliophysics Science Goals. While *Hinode* relates to all three, the observatory primarily addresses: **Explore the physical processes in the space environment from the Sun to the Earth and through the solar system**. Within the NASA National Research Council (NRC) Decadal Survey Priorities, *Hinode* targets: (a) Determine the origins of the Sun's activity and predict the variations of the space environment and (d) Discover and characterize fundamental processes that occur both within the heliosphere and throughout the universe.

In response to the 2012 NRC Decadal Survey Science Challenges and 2014 Heliophysics Roadmap Research Focus Areas, the *Hinode* mission has set forth four **Prioritized Science Goals (PSGs)**:

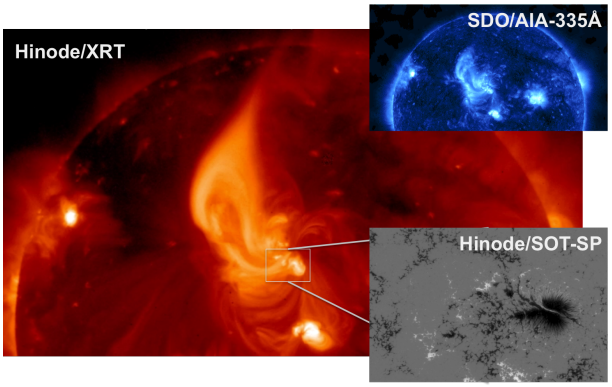

Figure 1: Hinode/XRT observes a large flaring region with a prominent cusp high into the corona, while SOT's spectro-polarimeter measures the underlying magnetic field. XRT's observations of the cusp extend far beyond those from Solar Dynamics Observatory's 335Å imager.

- Study the sources and evolution of highly energetic dynamic events.
- Characterize cross-scale magnetic field topology and stability.
- Trace mass and energy flow from the photosphere to the corona.
- Continue long term synoptic support to quantify cycle variability.

With three state-of-the-art instruments on board, the *Hinode* observatory operates as a coordinated unit with the additional capability to run instrument-specific targeted programs. This flexibility allows the mission to address the PSGs through a variety of operational programs such as: 1) Prioritized coordinated observations with the *IRIS* small explorer satellite and the *ALMA* radio ground-based observatory (GBO); 2) Focused observing campaigns for long-term target evolution; 3) Synergistic observations and Target of Opportunity campaigns with *SDO*, *RHESSI*, *NuSTAR*, *STEREO*, and various GBOs; and 4) Extended synoptic campaigns completing at least a solar cycle.

A significant change in Hinode status occurred in February, 2016, when the SOT Filtergraph (FG) camera failed after more than 9 years on-orbit due to an

electrical short circuit. The other two SOT cameras, the Spectro-Polarimeter (SP) and Correlation Tracker (CT) continue to work nominally. The loss of the FG camera means that no more broadband or narrowband images are available. In response to this failure, the telemetry previously used by the FG has been reallocated among the remaining instruments, nearly doubling that available for EIS and XRT; and more full-resolution rasters by SP (rare since the loss of X-band telemetry in 2008) and faster observing modes have been introduced.

Hinode's capabilities are highly synergistic with the full Heliophysics System Observatory (HSO). *IRIS*, the Interface Region Imaging Spectrograph, is particularly complementary with *Hinode* measurements as it is designed to provide spectra and images of the low atmosphere, which is difficult to properly survey without specifically-targeted instrumentation. With joint *Hinode* and *IRIS* data sets, we are able to investigate targeted regions from the photosphere, through the chromosphere and transition region, and out into the corona. Thus, great effort is put into coordinating these two resources.

Hinode also plays a significant role in joint observations with other NASA, HSO, and ground-based resources. Recurring examples include irradiance sensitivity studies between EIS and the Solar Dynamics Observatory's (*SDO*) Extreme-ultraviolet Variability Experiment (EVE), intercalibration between SOT and *SDO*'s Helioseismic and Magnetic Imager (HMI), and maturing coordination between XRT and the Nuclear Spectroscopic Telescope Array (*NuSTAR*) to understand AR thermal plasma distribution. *Hinode* has coordinated with 59 observatories, sounding rockets, and balloons and at least 69 different instruments, primarily via the Hinode Operation Plan (HOP) program. Several new opportunities will soon become available with the upcoming launches of Solar Probe Plus and Solar Orbiter and the first light of the Daniel K. Inouye Solar Telescope (*DKIST*).

Beyond the HSO and extensive GBO campaigns, *Hinode* also performs many independent investigations. The long baseline synoptic campaigns dating back to 2006 have given us valuable insight into cycle variability. *Hinode* has experienced an unexpectedly quiet maximum and the polar field reversal, and will witness the progression of the next cycle. *Hinode* is uniquely capable of sensitive, long term measurements of magnetic and high-energy solar variability.

Over 20 countries participate in the analysis of *Hinode* observations, contributing to major advances in our knowledge of the evolution of the photospheric magnetic field, coronal energy storage and release, and space weather. *Hinode* science data have been used in 1095 known refereed science journal articles and at least 123 graduate student theses.

The following sections outline recent mission successes and present the PSGs for the next extension period. These highlights are directly correlated to NASA priorities as outlined in the 2012 NRC Decadal Survey Challenges (DSCs) and 2014 Heliophysics Roadmap Research Focus Areas (RFAs).

2 RECENT RESULTS & FORWARD WORK

For each PSG, the following sections highlight selected results obtained using *Hinode* data since the previous Senior Review (∼2015 – present) and the forward work being proposed or already underway. These results are summarized in Table 1 and referenced against the relevant RFAs and DSCs from the Heliophysics Roadmap to clearly delineate how the mission goals reflect those of the SMD.

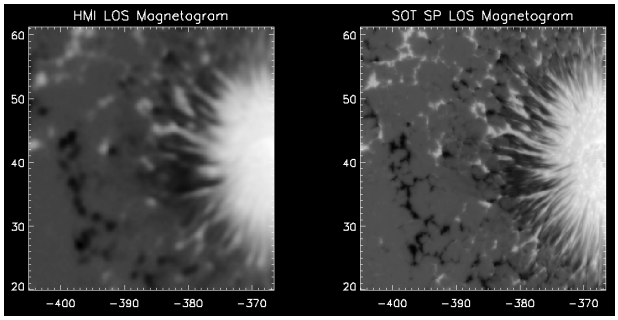

Figure 2: Comparison images between SDO/HMI (left) and Hinode/SOT-SP (right) magnetograms.

Although *Hinode* is still able to pursue all of its PSGs, there is scientific impact from the loss of SOT-FG. FG performed beautifully for 9 years and made many important discoveries (especially images of Ca II H of flare ribbons, prominences, and spicules) and sensitive magnetograms. Replacements for FG are lower resolution images from *SDO*'s Atmospheric Imaging Assembly (AIA) and *IRIS* slit-jaw images (always available for *IRIS* at only slightly lower resolution). Of course, imagery of similar or higher resolution is occasionally available from the best ground-

based observatories, and new ones with new capabilities are coming on-line (e.g., the Swedish Solar Telescope (*SST*)'s CHROMOspheric Imaging Spectrometer (CHROMIS) and *DKIST*).

Figure 2 demonstrates that SOT-SP continues to make vector magnetograms of excellent quality (spatial resolution, sensitivity, temporal uniformity, and absolute accuracy) that are unaffected by seeing or time of day, though high time resolution is only possible with tall, narrow fields of view. *SDO*/HMI vector magnetograms are available at lower resolution, and comparisons with SP (Sainz-Dalda et al., submitted) show they are indeed accurate in sunspots and dense plage but not so accurate in smaller-scale fields. Ground-based chromospheric magnetograms with high-resolution are beginning to appear, which have great promise to complement SP, HMI, and *IRIS*.

As mentioned in § 1, the silver-lining to this situation is the redistribution of the telemetry. Since the loss of the X-band in 2008, all on-board instruments have been sharing a very limited amount of bandwidth through the implementation of highly efficient operations. The large percentage of telemetry formally allocated to SOT-FG is now being utilized by the remaining instruments (SOT-SP, EIS, and XRT), paving the way for an updated observational paradigm including, but not limited to, more full-resolution SP rasters, more EIS line profiles, and opportunities for very high cadence XRT sequences. Additional telemetry is allocated to EIS and XRT during limb observing, opening the opportunity for high cadence coronal observations of erupting prominences. **By loosening the constraints on observatory science through this agility in telemetry redistribution, the *Hinode* team is able to stretch the limits of the observations to create new and unique data sets.**

2.1 PSG1 – Study the sources and evolution of highly energetic dynamic events.

One of *Hinode*'s primary missions is to observe flares at all scales, from the photosphere through the corona, spanning a wide range of temperatures at high resolution, and with unprecedented sensitivity to surface magnetic fields. To date, the mission has observed over 14,000 flares of various sizes, including a total of 710 M-class and 49 X-class flares. By taking advantage of the synergies available from complementary resources, *Hinode* has significantly contributed towards improving our understanding of the source of these dynamic events and their energetic capacity.

2.1.1 Large-Scale Eruptive Events

Hinode's success in capturing solar flares is owed, in large part, to targeted AR campaigns, well-tuned flare trigger responses, Focused Mode sequences, and coronal mass ejection (CME) watches. Large-scale eruptions, often associated with erupting flux ropes, give us the opportunity to observe the largest releases of energy in the solar system.

Hinode observations of flare ribbons, coupled with those from other instruments, provide evidence for an electron beam mechanism for flare energy transport. Gömöry et al. (2016) examined the EIS Fe XVI and Fe XXIII lines during the impulsive phase of a flare, and found insignificant downflows in the cooler line, strong upflows in the hotter line, and a strong increase in densities shortly after the flows were detected. These spectroscopic observations show that explosive evaporation occurred, even though the Reuven Ramaty High Energy Solar Spectroscopic Imager (*RHESSI*) indicated a comparatively low energy density in the footpoints. These results imply that the plasma response at the footpoints depends on the properties of the impinging electron beam.

The upflowing plasma resulting from chromospheric evaporation has given clues about flare energy transport. Imada et al. (2015) observed strong upflows during a flare in the Fe XXIII EIS line, but downflows in others. This observation is surprising since the flow reversal temperature is theorized to be much lower. The modeling accompanying this study indicates that these strong downflows at high temperatures

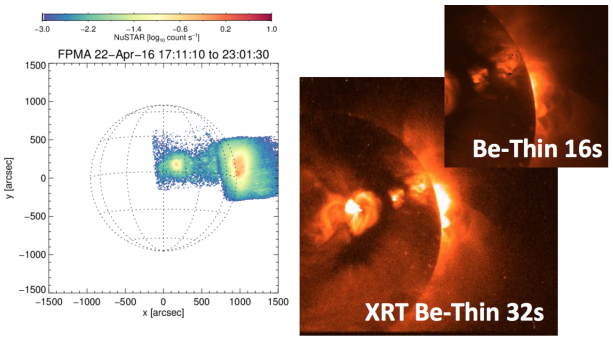

Figure 3: Coordinated observations between Hinode/XRT and NuSTAR on 2016 Apr 22 (courtesy of I. Hannah).

may be due to a suppression in the thermal conduction in the flare loop. Tian et al. (2015) also studied a pair of large flares, and found correlations between the blueshifted velocity in the *IRIS* Fe XXI line and the derivative of the soft X-ray (SXR) emission observed by XRT, indicating that there is a correlation between the velocity of the upflowing plasma in a flare and the energy deposition rate.

Understanding energy transport in solar flares has benefited greatly from the available suite of heliophysics spacecraft. The launch of the hard X-ray (HXR) astrophysics observatory, *NuSTAR*, adds an additional high energy dimension to our flare knowledge. *NuSTAR* has recently succeeded in imaging quiescent ARs with coordinated *Hinode* data sets (Figure 3, Hannah et al., 2016). The past few years of coordinating the two observatories have focused on creating viable data sets from *NuSTAR*, which is not optimized for solar viewing. Significant progress has been made on this front, and new results are anticipated in the coming years that will provide insight into flare scaling laws.

Forward Work

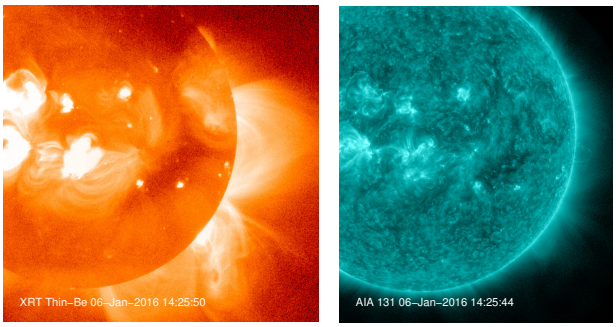

Figure 4: XRT Thin-Be image (left) and AIA 131 Å image (right) during a CME that originated from a source region behind the west limb. XRT detects structure out to the edge of its field of view, while AIA only sees some faint emission near the limb.

CMEs are clearly heated as they evolve (e.g. Lee et al., 2015), but the exact mechanism for this heating remains a mystery (Murphy et al., 2011). New full-Sun data sets provided by XRT's CME Watch program during Focused Mode will provide thermodynamic diagnostics of hot plasma during coronal mass ejections. Often events seen by XRT in this observing mode are faint in AIA, as shown in Figure 4. These data sets will enable the characterization of the evolution of CME heating as they leave the Sun, providing useful constraints on proposed heating mechanisms.

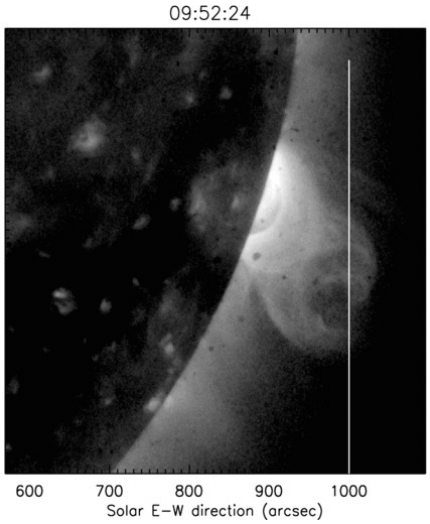

Figure 5: Position of the EIS slit (vertical line) for a behind-the-limb CME observed by XRT (Landi et al. (2010); Savage et al. (2010)).

A general science goal for observing flares and CMEs is to compare their measured physical characteristics, morphology, and evolution with current models developed to explain their origin and sources of heat and energy transport. The primary EIS goal during the rise phase of the next cycle will be to observe CMEs off-limb, taking advantage of the increased telemetry allocation for limb observations. The objective is to capture CMEs as they move through the EIS slit in Sit&Stare mode, as was done by Landi et al. (2010) to determine CME temperatures, line-of-sight (LOS) speeds, and electron densities (Figure 5). Complementary XRT observations of this CME were also analyzed by Savage et al. (2010) showing coronal flows that would not have been possible to observe had *Hinode* not been tracking the AR over the limb.

Long exposures are required by both instruments and the full EIS CCD should be read out to cover the wide range of CME temperatures. Observing CMEs close to the limb allows us to probe the elusive heating source(s). This phase of the eruption is simply not observable with typical coronagraphs due to the occulting disks and diffraction edges.

In addition to observing CMEs directly, it is im-

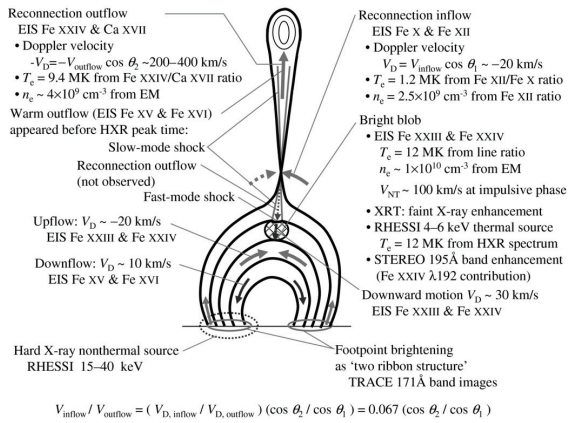

Figure 6: A side view schematic of the standard flare model. Important parameters for observation, referenced to the corresponding instrumentation, are shown with results from Hara et al. (2011).

portant to observe the pre-eruptive AR as completely as possible. The physical characteristics of flux ropes and the morphology of the AR provide important checks on theories for flux tube eruption. Recently Syntelis et al. (2016) have determined temperatures, upward motion speeds, and electron densities for flux ropes using EIS and AIA observations. Increasing the production of these data sets (i.e., EIS raster observations of ARs) is a near-term goal. Excellent examples of what can be achieved by *Hinode* XRT and EIS off-limb observations are published by Hara et al. (2008) and Hara et al. (2011) (Figure 6). On-disk flare observations will include SOT-SP measurements and will benefit from the increased telemetry for high resolution SP maps of the underlying AR magnetic fields as the sunspot evolves through an eruption. Combining the data sets with those available from AIA significantly reduces the impact from the loss of SOT-FG.

2.1.2 Small-Scale Eruptive Events

The heating of the non-flaring corona is likely dominated by small energy releases occurring at small spatial and temporal scales (e.g., Klimchuk, 2015). Observations of the spatial, temporal, and thermal structuring of the plasma from the solar chromosphere to the transition region (TR) and corona, combined with numerical models, can provide tight constraints to the nature (e.g., magnetic reconnection nanoflares vs. Alfvén wave heating) and properties of the heating mechanisms, and to the mechanisms of energy transport throughout the atmosphere (e.g., thermal conduction vs. non-thermal particles).

The amount of hot plasma ($\geqslant$4-5 MK, above the peak of the quiescent AR emission measure distribution) can provide stringent constraints on magnetic reconnection events (e.g., Reale et al., 2009). Recent studies have further explored the presence of hot plasma in a non-flaring AR (e.g., by combining EIS, XRT, and *SDO* data (Petralia et al., 2014), or by using expressly designed XRT observing sequences (e.g., Schmelz et al., 2016). Results suggest further evidence for the presence of minor very hot plasma components, pointing to some significant role of magnetic reconnection in the heating of ARs. Solar observations with *NuSTAR* have also provided stricter upper limits on the hot plasma (Hannah et al., 2016).

However, recent modeling efforts (e.g., Barnes et al., 2016a,c; Dzifčáková et al., 2016) have highlighted the multitude of physical effects (e.g., timescales of plasma response, ionization non-equilibrium, differential heating between electrons and ions) that severely complicate the diagnostics of the heating properties based on the plasma thermal distribution. Joint *Hinode-IRIS* observations (with *SDO* and *RHESSI*) have provided promising alternative diagnostics for coronal heating mechanisms by combining the coronal, chromosphere, and TR observations of hot coronal loops. Initial *IRIS* observations of an event showing TR variability at the footpoints of hot loops (i.e., moss), combined with RADYN numerical models, provided interesting indirect evidence of heating in the TR. This heating from non-thermal electrons associated with coronal magnetic reconnection provide constraints on the properties of non-thermal electrons (Testa et al., 2014).

Continued efforts for coordinations between *Hinode* and *IRIS* have yielded a sample ($\sim$10) of similar observations, where the full diagnostics can be exploited to investigate the relevance of thermal particles in these small AR heating events, and the properties of both non-thermal electrons and of nanoflares. The chromospheric/TR spectral observations (from *IRIS* and EIS) constrain the initial plasma response to heating release, while the coronal data (XRT and *SDO*/AIA) provide the necessary comparison for the coronal emission predicted by the models (and the assumptions on the non-thermal electron distributions

are checked against *RHESSI* data when available).

Significant improvements have been made to the models (Allred et al., 2015) to take into account important effects such as return current, background chromospheric heating, and non-equilibrium ionization (Allred et al. 2017, in prep., Polito et al. 2017, in prep.). These coordinated observations reveal the presence of non-thermal electrons in at least a fraction (∼25%) of the observed events (Testa et al. 2017, in prep.).

Forward Work

XRT is capable of taking very high cadence images, at 3 s cadences or faster. These high cadence image sets allow for the study of the high temperature heating mechanisms of small-scale solar brightenings, sometimes referred to as microflares (Lin et al., 1984). The exact heating mechanisms of microflares are uncertain, though they at least share many characteristics with large solar flares (Gary et al., 1997).

By detecting microflares with XRT and using the Enthalpy Based Thermal Evolution of Loops (EBTEL, Cargill et al., 2012a,b; Klimchuk et al., 2008) along with the genetic minimization algortihm PIKAIA (Charbonneau, 1995), Kobelski et al. (2014b) were able to show the necessity for multiple heating events, but were not able to fully determine the temporal structuring of the constituent heatings. The ability to distinguish the shape of the heating functions was limited, in part, by the cadence (∼ 25 s).

During initial testing in November of 2006, a series of high cadence XRT data sets were taken. Approximately 29 mins of data was obtained with the Thin-Be filter at a cadence of 6 s (including ∼3 mins at a 3 s cadence). Similar data was taken with the Med-Al filter for 90 mins at a 20 s cadence. At least 60 individual microflare events were readily detected in the 6 s cadence Thin-Be data (Figure 7), each of which are likely caused by a series of individual heating events (Kobelski et al., 2014). The triggering mechanism is crucial for understanding the flow of energy into the corona (Hudson, 1991; Ofman et al., 1995; Parker, 1988; Reale et al., 2009).

Because the analysis of this existing data set is limited by the lack of available coordinated observations, we need to plan new high-cadence, jointly-observed data sets to provide new insights into heating of the solar atmosphere. Coordinated observations at different layers of the solar atmosphere at similar spatial and temporal resolutions is necessary for tracking the energy deposition. With the current fleet of solar observatories, we will be able to better understand how these heating events are triggered.

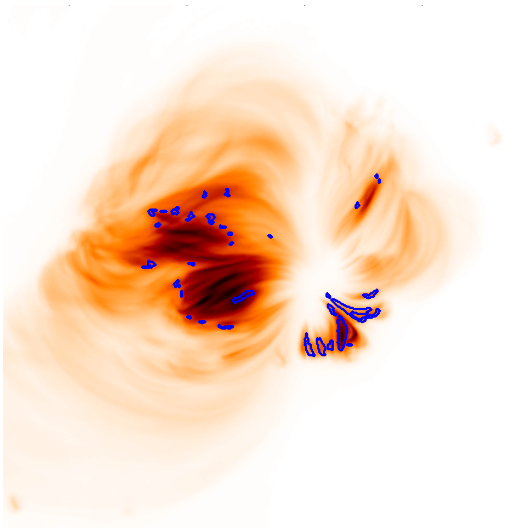

Figure 7: Median image of the 6 s cadence XRT Thin-Be observations on 2006 November 14. The blue contours outline the locations of microflares detected during the 29 min observations. The high cadence observations allowed the detection of a significant number of small features in the Eastern section of the AR.

The observations in Figure 7 are at wavelengths largely unaffected by filter contamination (Narukage et al., 2011; Takeda et al., 2016). Histograms applied to spot maps provided by `xrt_prep` (Kobelski et al., 2014b) show that 80% of the un-clean pixels experience less than a 1% deviation from the interpolated value when observing with the Thin-Be filter. When observing with the lower wavelength Al-mesh filter, more than 80% of the contaminated pixels experience notable deviations from their estimated value. We can thus assume that for filters thicker than Thin-Be, the spots continue to have minimal effect on the data, and it is possible to obtain similar observations to the 2006 test campaign while simultaneously obtaining coordinated support from instruments such as *IRIS*, *SDO*, and the Atacama Large Millimeter Array (*ALMA*).

The tools available to analyze these brightenings have improved since the works of Kobelski et al. (2014) and Kobelski & McKenzie (2014). An enhanced version of EBTEL has been created that in-

cludes the effects of a 2-fluid plasma with increased speed (Barnes et al., 2016b), which will greatly improve upon previous results.

2.1.3 Flux Transfer & Magnetic Reconnection

A primary manifestation of energy transfer in the corona is the heating of flare loops and erupting flux ropes. Guglielmino et al. (2016) studied a C4.1 flare and found that the bulk of the X-ray emission occurred in the δ-spot region, where plasma is on the order of 20 MK. Nindos et al. (2015) did a survey of hot flux ropes in CMEs as observed by the AIA 131 Å channel and found that almost half of CMEs have a hot flux rope structure. Supplementary XRT data was very important to this study, as it showed that this number is only a lower limit, since some hot flux ropes can be observed by XRT but not AIA. Reeves et al. (2015) found direct evidence for reconnection in a small eruption observed with *IRIS* and AIA. Hot loops were observed by XRT after the reconnection, indicating that heating had occurred in the plasma in these loops. These loops were difficult to observe in AIA because neither the 94 Å nor the 131 Å passbands were very sensitive to their temperatures.

Critical to our understanding of flare energy transport is a consistent picture of how particles, particularly electrons, are accelerated during reconnection. Observations of electron beam properties need to take into account both chromospheric energy deposition as well as dynamical effects such as erupting filaments and surges. The properties of a surge during a large flare were investigated by Doschek et al. (2015a) using *Hinode* (EIS & XRT), *RHESSI*, and *SDO*. The results strongly indicate the need for complex, multi-threaded loop structures to be included in standard flare models as current models were insufficient.

Conversely, electron beam properties from the weaker end of the spectrum were studied by Warren et al. (2016) and Reep et al. (2016), combining EIS, *RHESSI*, and *IRIS* data to study the properties of a small flare. The *IRIS* Si IV line measurements indicate the temperature at which downflows begin. Modeling has shown that this temperature is a function of the low energy electron beam cutoff – an important unknown property of high energy particles in solar flares. Warren et al. (2016) measured the flow properties of the Si IV line and found that downflows occurred over extended times, which is not predicted by models that assume an impulsive high energy input. The modeling of this event used EIS and *RHESSI* to determine the properties of the coronal portion of the flux tube model. It became clear that the *IRIS* data could only be explained if the flux tube contained many unresolved strands (nanoflares) (> 60) below the resolution of a single *IRIS* pixel. This exciting result places a constraint on the sizes of nanoflare magnetic strands.

This complexity of the electron beam interaction with explosive chromospheric events is under continuing investigation. Doschek et al. (2016) determined electron densities in explosive events seen in Si IV *IRIS* spectra and obtained high values from about 10^{11} to 10^{12} cm^{-3}. The new technique developed for these density derivations is a way to measure very high densities in flares, which is critical information for modeling either coronal conduction or electron beam heating of the chromosphere. EIS data provide the coronal electron flare densities, complementing the *IRIS* chromospheric data.

Forward Work

The simple topology of coronal jets will serve as a useful laboratory for probing energy release during the reconnection process. Studying the acceleration mechanism in jet spires can lead to an understanding of the energy transfer process during reconnection. Matsui et al. (2012) used EIS to examine the velocity of the plasma in a jet spire and found that it increased roughly as a function of temperature. This finding indicates that the plasma in the jet is accelerated by a chromospheric evaporation mechanism. We will examine many jet observations taken during Focused Mode AR runs in order to understand how prevalent this acceleration mechanism is, and if "standard" jets have different acceleration mechanisms than "blowout" jets (e.g. Moore et al., 2010). The combination of XRT, EIS, AIA, and *IRIS* will be invaluable for this study, as this combination of instruments will provide plane of sky and LOS velocities over a broad range of temperatures.

2.2 PSG2 – Characterize cross-scale magnetic field topology and stability.

Hinode's broad coronal temperature coverage and sensitivity to surface magnetic fields make the observatory ideally suited for tracing the evolution of mag-

netic structures across spatial scales and measuring their effects on solar magnetic variability.

2.2.1 Active Regions

Hinode/XRT observations of hot loops best visualize the non-potential fields in solar ARs. Non-potential fields are extremely important both for storing magnetic free energy and for releasing it to power flares and CMEs. XRT's observations of AR loops have proven the best at constraining non-linear force-free field (NLFFF) models of the coronal magnetic field using the flux rope insertion method (Savcheva et al., 2012a; van Ballegooijen, 2004). The method is based on magnetofrictional relaxation of a flux rope inserted in a potential arcade and, as such, it does not require NLFFF equilibrium to be reached. Hence, regions close to moments of eruption can be modeled with this technique, making this method highly unique.

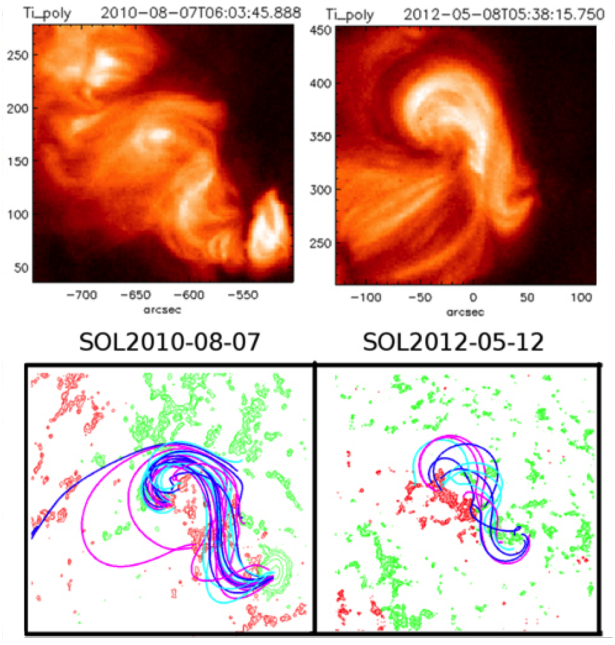

Figure 8: **Top***: XRT images at the time of the magnetic field models.* **Bottom***: Field lines traced from the corresponding best-fit marginally stable models for the three regions (Savcheva et al., 2016).*

Savcheva et al. (2016, 2015) and Janvier et al. (2016) modeled eight regions in total just before their eruption, using XRT and AIA data to constrain the hot pre-eruption loops (Figure 8). The free energy content, helicity, and poloidal and axial fluxes in the flux ropes were estimated in the best fit models matching the time just before any flare-related features appeared. Then slightly unstable models were obtained by adding a unit of axial flux to the best-fit marginally stable models and the formation of an inverted-teardrop shaped flux rope was observed (Savcheva et al., 2012a,b).

The field topology computed from these models showed that a hyperbolic flux tube (HFT; Titov et al., 2002) appears under the flux rope, where reconnection takes place in the magnetofrictional evolution and the configuration changes in response. The HFT is a self-crossing of the quasi-separatrix layer (QSL) that wraps around the flux rope and separates it from the overlaying field. Savcheva et al. (2015) showed, for the first time observationally, that the feet of the HFT intersect the photosphere at the location of flare ribbons in all studied flares, which is direct evidence of the standard 3D flare model (Aulanier et al., 2012; Janvier et al., 2013).

Savcheva et al. (2016) further showed that as the magnetofrictional evolution proceeds, the HFT feet spread and the overlying QSLs move apart together, as in the AIA observations. While these features were demonstrated for mostly classical two-ribbon flares in Savcheva et al. (2016, 2015), the same correspondences were outlined for the circular ribbon X-class flare containing a sigmoid (Janvier et al., 2016). The AIA ribbons, QSLs based on the pre-flare magnetic field models constrained by XRT and AIA data, and the vertical current density distributions derived from vector HMI magnetograms all match each other, further confirming the standard 3D flare model.

These studies successfully pointed out that NLFFF models heavily constrained by coronal observations (mainly by XRT) have predictive power in the sense that models constructed to match purely pre-flare observations, when rendered unstable, reproduce a range of flare and post-flare features with high accuracy and in qualitative as well as quantitative aspects.

These conclusions prompted the use of XRT-constrained, unstable models as the initial conditions to a series of data-constrained magnetohydrodynamic (MHD) simulations. These models focus on the eruption onset and globally investigate the CME propagation in the corona and interplanetary space. These studies are underway and are on the forefront of solar physics research.

Further use of NLFFF extrapolations of photo-

spheric vector fields to infer the coronal magnetic field has been studied once again by the "NLFFF consortium" led by DeRosa et al. (2015). Vector fields of an isolated AR, measured with different spatial resolutions were extrapolated using 6 different methods (9 extrapolations in all), and compared using various characteristics including free energy, relative helicity, and accuracy of force-free and divergence-free conditions. The results differ widely among the various methods, reinforcing the conclusion that extrapolations must be compared with coronal images (XRT and AIA) to have credibility and that numerical results from them should be treated with caution.

SOT-SP maps have also been used to study the emergence of helicity in ARs. Seligman et al. (2014) made an exhaustive study comparing magnetic helicity in the photosphere (from 2440 SOT vector magnetograms) with subsurface kinetic helicity (from GONG and *SDO*/HMI helioseismic ring diagrams). Two proxies for magnetic helicity were used: current helicity and twist. The well-known hemispheric bias in magnetic helicity was seen for strong field regions (sunspots and pores) and kinetic helicity below the ARs, with the same sign of the regression line for latitude dependence.

Somewhat surprising was their finding of no significant region-by-region correlation between the two, although annual averages of both show the same cycle variation. This finding suggests that either the helioseismic estimates of subsurface flows still do not have enough resolution to capture the dynamics of AR fields, the rise through the convection zone randomizes the effects on the individual flux ropes that form ARs, or the helicity estimates are incorrect.

The situation is further confused by Koch-Ocker & Petrie (2016), who measured the helicity proxies in 179 ARs by selecting one SOT observation closest to central meridian for each one. These results did not show the hemispheric bias at all, and opposite signs were found for strong and weak fields; both results were shown to be robust in simulations of added noise and blurring. Similar perplexing results were found using a different technique on HMI data by Zhang et al. (2016), a result that will be tested with the higher resolution SP data.

Forward Work

Rapid progress is being made toward our understanding of AR magnetic structure. *Hinode* SOT and XRT observations continue to provide the critical boundary conditions for models and simulations. During the next 2-3 years, several groups around the world will be developing and evaluating data driven MHD simulations of AR evolution. Over the declining phase of the solar cycle, there will be long periods when only a single AR appears on the disk. Long duration *Hinode* observations will provide ideal data sets to develop these 1st generation codes. The SXR wavelength region observed by XRT is dominated by Fe XVII emission lines in ARs. These lines are the strongest and dominate the radiative cooling of the AR. As a result, XRT images show the transient non-potential structure of an AR better than any of the AIA passbands. SOT-SP remains the standard for photospheric vector magnetic field measurements.

Hinode adds to our ability to measure the topological features from magnetic models of ARs. Current layers, QSLs, and regions with large Lyapunov exponents should correspond to variations in plasma properties - temperature, density, velocity, non-thermal widths. Detailed comparisons with EIS constrain the role of large scale topological structures on the plasma heating problem. As data driven and data constrained simulations develop, it is critical for instrument teams to provide timely and relevant data products to scientists with computational backgrounds. The *Hinode* team has an excellent track record of working with the modeling community.

2.2.2 Small-Scale Magnetic Fields

The weak "internetwork" (IN) fields of the quiet Sun (QS) contain a huge amount of magnetic flux at all times, comparable to the total flux in network regions and within an order of magnitude of the total to emerge in ARs in a solar cycle. Earlier *Hinode*/SOT observations showed that some fraction of the IN flux reaches chromospheric heights after emergence (Martínez González & Bellot Rubio, 2009), becoming visible in Ca II H images, suggesting that IN fields may play an important role in energy transfer to and heating of the upper atmosphere.

Recent analyses of SOT data have clarified two basic IN properties which have been controversial, their geometric structure (isotropic vs. horizontal) and emergence and disappearance rates (uncertain until now by $\sim$2 orders of magnitude). Lites et al.

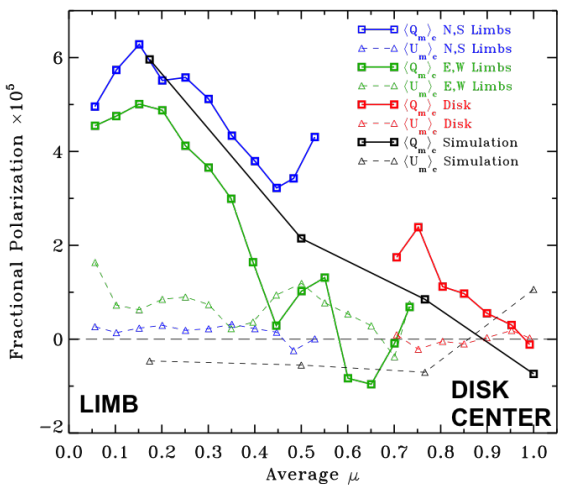

Figure 9: Change in polarization of IN fields with inclination angle, indicating that the weakest component of QS magnetism is dominantly horizontal (Lites et al., 2017).

(2017) studied the center-to-limb variation of calibrated Stokes profiles to determine whether horizontal fields predominate over vertical, without the model-dependence of inversion techniques. They found clear evidence for horizontal fields (Figure 9), in agreement with MHD simulations, which they analyzed in identical fashion to validate the technique.

Gošić et al. (2016) measured the emergence rate to be $120 \pm 3\,\mathrm{Mx\,cm^{-2}\,day^{-1}}$ and the disappearance rate to be essentially identical. At this rate, IN fields emerge as much flux as in all ARs in a cycle in 3 days, and they can replace the entire network flux in 10 hours. IN fields disappear by interaction with network features (40%), simply fading away (40%), and cancellation (20%). Several joint *Hinode-IRIS* observations have been made to assess the chromospheric consequences of the first class of interactions and these will continue in the next few years.

Forward Work

A number of *IRIS-Hinode* Operational Plans (IHOPs) have been and will continue to be run to address the difficulty of assessing chromospheric effects of weak IN fields in QS and plage. Gosic et al. (in prep) have looked at the effect of magnetic cancellation on the overlying chromosphere with *IRIS* and find little evidence for heating. However, during the emergence process, interaction with overlying fields is inevitable, and many more IN elements disappear by interacting with the strong network flux concentrations than by cancellation. Recent simulations by Martinez et al. (submitted) show that ambipolar diffusion allows the IN fields to diffuse through the chromosphere, where interaction with pre-existing fields leads to heating and jet acceleration. We plan to use rapid, coaligned SOT-SP scans with simultaneous *IRIS* observations in a variety of quiet and active target regions to search for direct observational evidence for these processes. Joint campaigns with *ALMA* and the new SST instrument, CHROMIS, will provide high-resolution Ca II K line profile images; eventually, joint campaigns with DKIST will also be performed.

The SOT technical section describes several improvements that are being made to such joint observations, including faster SP observing modes, improved pointing accuracy to increase the chances of overlapping SP and *IRIS* slit rasters, production and distribution of datacubes of SP measurements with accurate pointing information, and cubes of SOT images coaligned with *IRIS* and readable with *IRIS* analysis tools.

2.3 PSG3 – Trace mass and energy flow from the photosphere to the corona.

Probing energy transfer in the low solar atmosphere is notoriously difficult due to poorly understood ion behavior at such extreme transitions, yet this region is critical to target as it supplies mass to the solar wind and heat via particle flux and waves.

2.3.1 Solar Wind

EIS measurements have established that the plasma composition of the AR outflows is the same as that measured *in situ* in the slow solar wind by the Advanced Composition Explorer (*ACE*) (Brooks et al., 2011). The global magnetic field topology is not always consistent with this picture, however. The AR studied was completely covered by a helmet streamer, and in a study of seven ARs, Edwards et al. (2016) showed that most do not have extended field in the vicinity of the outflows. Only in one case, adjacent to a coronal hole (CH), was an outflow channel found.

Open field in the form of CHs adjacent to the closed AR field may play an important role in the

outflow process (Fazakerley et al., 2016), so large-scale field of view observations are increasingly important. Since 2013 EIS has taken occasional full Sun slit scans to construct source maps from a combination of magnetic field modeling, Doppler velocities, and plasma composition measurements. These maps, which complement the full Sun slot scans taken every three weeks, show that a large fraction of the *in situ* mass loss rate can be explained by outflows on open field associated with ARs (Brooks et al., 2015). Only a small fraction of the closed potential field needs to be open to explain all of the mass flux, implying that a combination of global scale observing and complex magnetic field modeling will improve our understanding of the connection between AR outflows and the heliosphere.

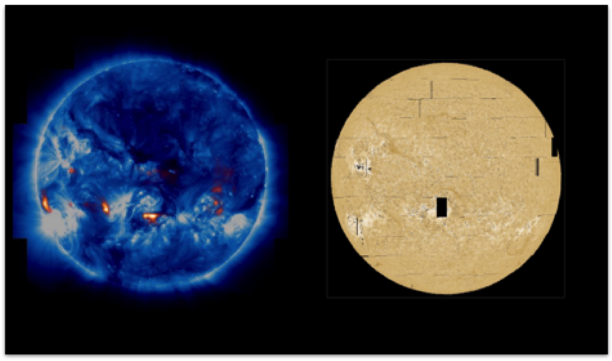

Figure 10: Slow solar wind source map (left) constructed from an EIS mosaic taken in October 2015. The red sources are areas where plasma with a slow wind composition is outflowing on open magnetic field lines (from a potential field source surface (PFSS) extrapolation). The sources are overlaid on an AIA 193 Å composite intensity image. Mg II *reversed core intensity from an IRIS mosaic (right) taken close to simultaneously with the EIS scan.*

Since 2015 these full Sun scans have also been coordinated with *IRIS* (Figure 10), which extends the spectral coverage to the chromosphere where potential drivers, such as jets, originate. The EIS observations have now been developed to increase the spectral coverage by a factor of three, which allows a significantly improved diagnostic capability including, cooler temperature lines from Mg V-VII & Si VII that help to bridge the temperature gap to *IRIS*, and S XIII and Fe XIV lines that allow full disk mapping of ion temperatures in addition to electron temperature.

In 2015 analysis of EIS flare spectra revealed the existence of small regions near sunspots that exhibit an inverse first ionization potential (FIP) effect (Doschek et al., 2015a). The FIP effect indicates the composition of the plasma and can be used as a proxy of its source (coronal vs. photosphere). This measurement is the first instance of the inverse FIP effect in the Sun (Figure 11), although it is seen in stars with large starspots. Sunspots by comparison are nano-starspots. In 2016 this discovery was reinforced by additional flare spectra and many more spectral lines of argon (Ar) (Doschek & Warren, 2016). Recently, it has been found that the FIP effect can be stifled near sunspots over large areas of an EIS AR raster, resulting in composition measurements that fall between being purely coronal and photospheric. This exciting result calls into question the variability of the coronal composition in different types of solar regions, particularly near sunspots.

Forward Work

EIS is currently the only operating instrument with coronal composition spectroscopic diagnostic capability. To exploit this uniqueness, studies of fast solar wind sources and AR outflow composition are now emerging. Discrete features in polar CHs such as plumes, inter-plume lanes, and X-ray jets have been analyzed (Guennou et al., 2015; Lee et al., 2015). All of these features appear to have a fast wind-like photospheric composition. The jets, in particular, are consistent with the emerging flux reconnection model, where photospheric flux emerges, reconnects with the overlying open-field, and is rapidly ejected into the fast wind. Future EIS observations will determine which of these features is the dominant source of the mass flux of the fast solar wind.

A related new project will be to investigate the solar abundances in periodic density structures seen high in the corona in *STEREO*/COR2 observations near streamers. Viall & Vourlidas (2015) and Brooks et al. (2015) suggest that some fraction of the slow solar wind mass flux comes from high coronal regions, so far not examined by EIS. The results depend on whether these structures can be seen at the uppermost heights achievable by EIS. Preliminary investigations indicate that a statistically significant signal can be found in the S X line, and new coordinated EIS/*STEREO* observations are being planned.

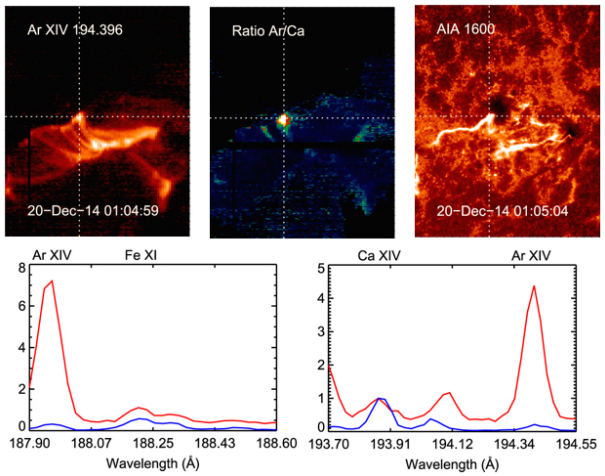

Figure 11: EIS observations of an inverse FIP effect. **Top***: a) An EIS image in the indicated wavelength of the high FIP Ar* XIV *line. b) The ratio of the Ar* XIV *line to a low FIP Ca* XIV *line formed at the same temperature. The bright spot shows that in this small region the ratio, which indicates an inverse FIP abundance, is much larger than in the surroundings. c) The AIA data show the location of the region and the sunspots in the AR.* **Bottom***: Spectra of Ar* XIV *lines relative to low FIP Ca and Fe lines. (Red – inverse FIP region; blue – expected coronal abundance; Doschek et al. (2015b)).*

The inverse FIP effect results will also be further investigated. Current work indicates that relatively large areas near sunspots can have abundances that vary between photospheric and coronal abundances, and sometimes an inverse FIP effect appears in a smaller area. To further solidify these results, composition measurements will be undertaken via large raster scans near sunspots to investigate changes in the solar abundances over larger areas than possible so far because of telemetry constraints during most of the mission to date. The rasters in the current EIS full-CCD database (used for the work up to now) generally have fields of view that leave out substantial areas of the regions around sunspots. Multiple smaller rasters with slightly different pointings could also be used. Of particular interest is the S line, used for our slow solar wind work, because it is a borderline high FIP element. These results are very current and need to be substantiated, but are so far consistent with predictions of the Laming (2015) model.

Additional progress since the last Senior Review has shed new light on solar abundances and the FIP effect which results in different photospheric and coronal abundances. Abundances are photospheric in high speed solar wind streams, and coronal in the slow speed solar wind. However, new observations (e.g., Landi & Testa, 2014; Shearer et al., 2014) have indicated that abundances may vary over the solar cycle *in situ* in the solar wind and in coronal streamers, and contain additional variations that had been indicated in earlier Solar Maximum Mission (*SMM*) observations of quiescent ARs but not fully appreciated until now (e.g., Schmelz et al., 1996).

Motivated by these recent results, we will start a new observing program to measure the coronal solar abundances through the current solar cycle. While EIS already runs several synoptic programs available to study cyclic abundance variations in the equatorial regions associated with the slow wind, there is no dedicated program monitoring abundances in the polar regions where the fast wind originates. We will add the appropriate diagnostics to the monthly *Hinode* polar monitoring campaign. S X has been the key high FIP ion used so far in EIS slow wind studies. We will attempt to use an Ar XI line to help substantiate the S results. S is a borderline high FIP element, but Ar is well into the high FIP regime. This increase in understanding abundance variations should improve tracking of the solar wind by using abundances as a diagnostic of the source regions.

2.3.2 Chromospheric heating

Understanding chromospheric heating is an important problem for both solar and stellar physics, but it is difficult because of the fine-scale structures involved, the many scale heights of density spanned, and the optically thick, non-LTE (local thermodynamic equilibrium) formation of the most accessible spectral lines. Since *Hinode* has limited chromospheric diagnostics alone, joint observations with *IRIS* and guidance from advanced MHD models are essential for making progress.

One of the first Ph.D. theses to be based on *Hinode* and *IRIS* observations is that of Skogsrud et al. (2015), who studied simultaneous spicule images at chromospheric and TR temperatures from SOT Ca II H, *IRIS* Mg II, C II, and Si IV, and AIA He II. The study found clear evidence for heating in some spicules, with TR images appearing later and higher than the

cooler bands. Synthetic observables from the BiFrost simulations show good agreement, including heating to TR temperatures. Brady & Arber (2016) also used SOT Ca II H spicule images for comparison with their models of wave heating and spicule acceleration.

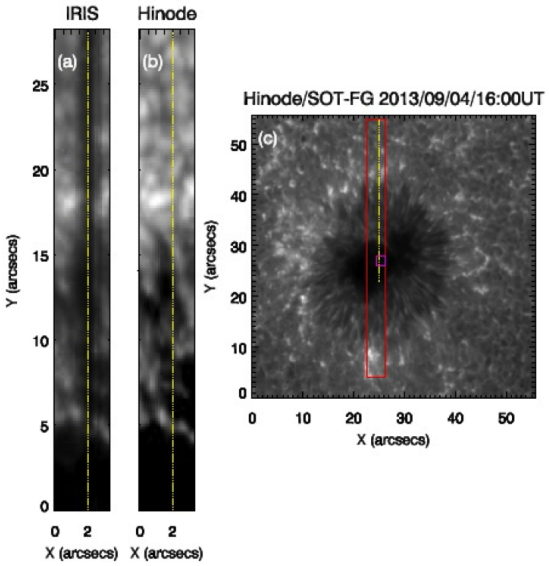

Figure 12: Hinode and IRIS observations of a sunspot used to trace upward energy flux via MHD waves into the chromosphere (Kanoh et al., 2016).

Another *Hinode-IRIS* (Masters) thesis is that of Kanoh et al. (2016), who used *IRIS* and SOT-SP observations to derive the upward energy fluxes in a sunspot umbra at photospheric and lower TR heights (Figure 12). They concluded that the waves were standing slow-modes in the photosphere, with propagation into the chromosphere and TR, where they presumably become shocks. Enough energy is dissipated in the chromosphere to contribute significantly to its heating in the umbra, but not enough appears to reach the TR to be significant for coronal heating.

A very different approach to the photospheric input to chromospheric and coronal heating was taken by Welsch (2015), who estimated the energy flux produced by granulation-scale shuffling of magnetic footpoints in a unipolar plage region. He measured horizontal velocities by correlation tracking of SOT-FG (NFI) magnetograms and combined those with vector magnetic fields from SP to estimate the vertical component of the Poynting vector. The flux measured on this timescale of several minutes was highly variable with both signs, but the average was upward and easily sufficient for coronal but not chromospheric heating. No obvious correlations with chromospheric activity were evident beyond the usual bright network in Ca II H, and it is clear that future work will need to use simultaneous *IRIS* and/or *ALMA* data to connect the photospheric boundary condition with the dynamics of the chromosphere.

Forward Work

Possible contributions to chromospheric heating by emergence and interaction of weak photospheric fields have been discussed in § 2.2.2. The same observing programs will be used in plage and ARs, with SP providing the best photospheric boundary conditions for analysis of *IRIS*, *ALMA*, and ground-based observations. An exciting new development is the inversion code of de la Cruz Rodríguez et al. (2016) that can construct a model atmosphere from the *IRIS* Mg h & k line spectra from the mid-photosphere to the TR. The code can potentially incorporate other observations, such as SP polarized spectra, to recover the complete atmosphere including magnetic fields, or *ALMA* microwave continua, to give more accurate upper chromospheric structure. With this tool supplementing the previously developed *IRIS* diagnostics, analysis of our coordinated observations should fully characterize the energetic contributions of chromospheric magnetic interactions and waves.

Recently, observations with *ALMA* have begun providing unique insights into the flow of energy through the solar atmosphere. Cycle 4 of *ALMA* observations began in October 2016, which is the first *ALMA* cycle officially supporting scientific solar observations (Kobelski & *ALMA* Team, 2016). The solar *ALMA* observations are taken in discrete bands at millimeter wavelengths which primarily detect thermal bremsstrahlung (Wedemeyer et al., 2016) and serve as a sort of linear thermometer of the chromosphere. The sub-millimeter wavelength regime provides unique solar observations, which are currently only accessible via high altitude radio interferometry, such as that provided by *ALMA*.

Vitally important to *ALMA* observations is supporting co-temporal data from coordinating instruments. SOT provides high resolution photospheric magnetic field context observations from below the chromospheric layers seen with *ALMA*, XRT provides high cadence observations (Section 2.1.2) of

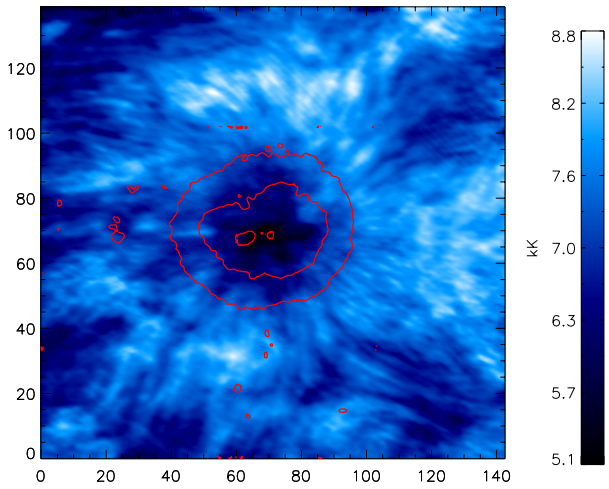

Figure 13: ALMA band 6 image mosaic utilizing 149 pointings of a sunspot from 2015 December 18 from ∼19:11 to 20 UT. Contours of the magnetic field strength (at 1100, 1750, and 2500 G) were obtained with SOT-SP and calibrated using Community SP Analysis Center (2006). Preliminary data show strong temperature gradients around solar ARs. The labels are in arcseconds.

the hot plasma in the corona above *ALMA* observations, and EIS provides spectroscopic context of the corona. *Hinode* supported *ALMA* test campaigns in 2014 and 2015 and has continued to support and coordinate with *ALMA* solar observations to make complete use of this unique observatory.

Figure 13 shows data from a sunspot as viewed with *ALMA* band 6 (∼239 GHz, 1.25 mm). The radiation at this wavelength originates from a region approximately 730-1000 km (Loukitcheva et al., 2015; Wedemeyer et al., 2016) above the photosphere at a temperature of ∼7000 K. The red contours are the magnetogram data from the SOT-SP, and can be traced through the chromosphere with *ALMA* and *IRIS* into the corona, where EIS and XRT provide spectroscopic context and high temperature thermal information in the corona, respectively.

The options for *ALMA* solar observations are currently limited to continuum observations at 100 and 230 GHz with spatial resolutions as high as 1.5" and 0.6", respectively. *ALMA*'s capabilities are continually being advanced as more of the telescope commissioning is completed. Current work is being done to increase the number of wavelength bands available for solar observing as well as the commissioning of solar spectroscopic observations. These updates will provide improved understanding of stratification within the chromosphere and potentially allow the observation of solar recombination lines (Wedemeyer et al., 2016). Ongoing improvements in the calibration of the antennae, commissioning of the correlator, and a full understanding of the phase shifts inherent within the system will allow higher spatial resolution as well as the measurement of all four Stokes parameters, which should enable measurement of the chromospheric magnetic field.

As the capabilities of *ALMA* solar observations improve, coordination with *Hinode* will allow full utilization of the data to track energy transfer through the chromosphere. The spatial resolution of the maps available from SOT-SP will soon be matched in the chromosphere with *ALMA*, and EIS and XRT provide unique coronal counterpart context.

2.3.3 Magnetic Waves

Developing a better understanding of plasma motions within the dynamically-structured corona is essential in addressing the coronal heating problem. One of the leading theories behind this problem is wave heating, wherein the plasma flows within and between coronal loops resulting in the generation, propagation, and dissipation of waves. The presence of the coronal magnetic field, coupled with large density variations, strongly alters the wave characteristics.

Many observations over the last 15 years (since *TRACE*) have shown that the entire solar atmosphere is filled with both propagating and standing MHD waves. AR loops, QS spicules, prominence fine structures, and CH jets and plumes have all shown waves in imaging and/or spectral observations. The dissipation of these waves by the resonant absorption mechanism has been studied theoretically, and indirect evidence from imaging instruments has been claimed to support it (Figure 14). A combination of SOT and *IRIS* observations, combined with advanced MHD modeling, has provided the first direct evidence for resonant absorption and associated heating to TR temperatures. Okamoto et al. (2015) observed coherent transverse oscillations of prominence threads with SOT and Doppler shifts from *IRIS* with a telltale phase difference to identify the mechanism; line intensities and widths from *IRIS* confirmed heating to (at least) TR

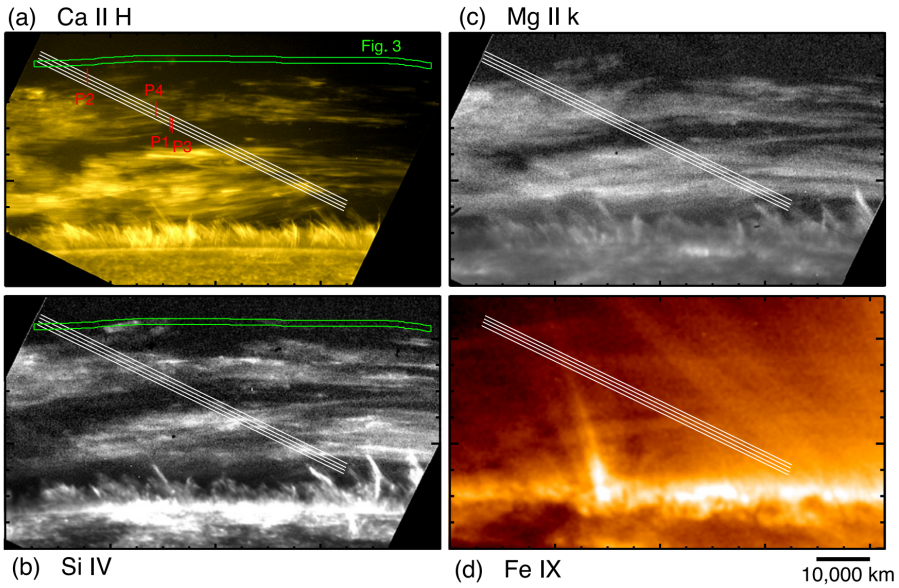

Figure 14: Snapshot of (a) Hinode/SOT-FG, (b) & (c) IRIS, and (d) SDO/AIA data sets used to derive evidence for resonant absorption heating by magnetic waves in the lower solar atmosphere (Okamoto et al., 2015).

temperatures, increasing with height. A detailed interpretation in terms of Kelvin-Helmholtz instabilities at the boundaries of oscillation threads (Antolin et al., 2015) matches the observations quite well.

EIS is unique in providing measurements of spectral line broadening of AR loops (Tripathi et al., 2011; Warren et al., 2011). The interpretations of EIS line broadening include waves as well as non-thermal energy dissipations that preserve ions at a larger temperature than electrons. In coronal loop studies based on wave heating, modeled non-thermal line broadenings have been compared to the results from EIS observations by creating maps of the intensity, velocity, and line width (Asgari-Targhi et al., 2014). The EIS non-thermal line velocity observations predict transverse velocities with respect to the loop axis on the order of 10-20 km/s. More sophisticated methods are under development to enable the study of wave propagation in a more realistic model of solar coronal loops in order to better compare with EIS observations.

Forward Work

Detailed modeling of MHD waves in the solar atmosphere has progressed tremendously during the 1st decade of *Hinode* observations. Constraining the properties of waves requires joint observations from *Hinode*, *IRIS*, and *SDO*. Over the next 2-3 years, scientists will develop more sophisticated models of coronal loops including the interactions between neighboring flux tubes in the photosphere, chromosphere, and the corona. This enhancement will allow for the study of wave propagation with a more realistic model of coronal loops, thus enabling more appropriate comparisons with observations.

The interesting study by Kanoh et al. (2016) discussed in § 2.3.2 focused on MHD waves in a sunspot umbra using only Stokes I and V to derive fluctuations in the LOS component of the magnetic field, following the method of Fujimura & Tsuneta (2009). Future observations and analyses will use longer time series and the full vector field from inversions (in sunspot umbra, penumbra, and pores) to clarify the nature of the wave modes involved. Oscillations in field strength have not yet been observed, and fluctuations in inclination and azimuth analyzed at different aspect ratios (disk positions) should also be sensitive indicators of the different modes. With simultaneous *IRIS* or ground-based observations (e.g., *SST* CHROMIS & CRISP or the Dunn Solar Telescope's (*DST*) IBIS instrument), mode conversion and chromospheric heating can be probed. New diagnostic capabilities for the *IRIS* chromospheric lines can provide velocities with some height resolution above the photosphere. Phase relations with different *SDO*/AIA channels may also reveal upward propagation.

2.4 PSG4 – Continue long term synoptic support to quantify cycle variability.

Hinode is well-equipped for monitoring variations in solar cycle evolution through long-term synoptic campaigns measuring proxies such as solar irradiance. Understanding the origin of our own Sun's dynamo, which powers the entire heliosphere, is applicable to stellar behavior throughout the Universe.

2.4.1 Solar Irradiance

The extended *Hinode* mission span, and wide range of observing wavelengths, are advantageous for long baseline measurements contributing to understanding solar irradiance variations. *SDO*/EVE measurements stop short of the true solar minimum, and the *TIMED* missions's Solar EUV Experiment (SEE) measurements below 270 Å are derived from broad-band photometer observations and CHIANTI spectra. It is necessary to know how the instruments' calibrations vary throughout that time frame. Towards this end, both EIS and XRT maintain databases of sensitivity degradation for calibrating the observations. The HOP 130 observations, repeatedly run throughout the *Hinode* mission, are useful for monitoring the EIS calibration. The most recent data demonstrate that the degradation in the EIS long-wavelength channel has saturated; these findings motivate revisions to the EIS calibration routines, which have previously assumed continued, exponential decay.

Simultaneously, XRT full-disk solar images obtained twice daily since the beginning of the mission yield a profile of SXR irradiance from 2008 to the present. The filter-ratio temperatures and emission measures obtained from the disk-integrated signals have been used to synthesize the disk-averaged solar spectrum, and to derive the irradiance in physical units of W/m^2. Analysis shows that the XRT irradiance calculated for the 110 Å wavelength range is in good agreement with the published *GOES*/X-Ray Sensor (XRS) flux in 18 Å, for the period of Jan 2010 through May 2012. For the cycle-minimum period 2008 to 2010, the solar X-ray flux was below the XRS detection limit, and the XRT irradiance is actually more reliable. However, for the period after May 2012, XRT experienced a calibration shift due to partial failure of a pre-filter. Current efforts include correction to the XRT response function by leveraging the observation so that the XRT-derived irradiance varies in parallel with that obtained from the *GOES*/XRS flux.

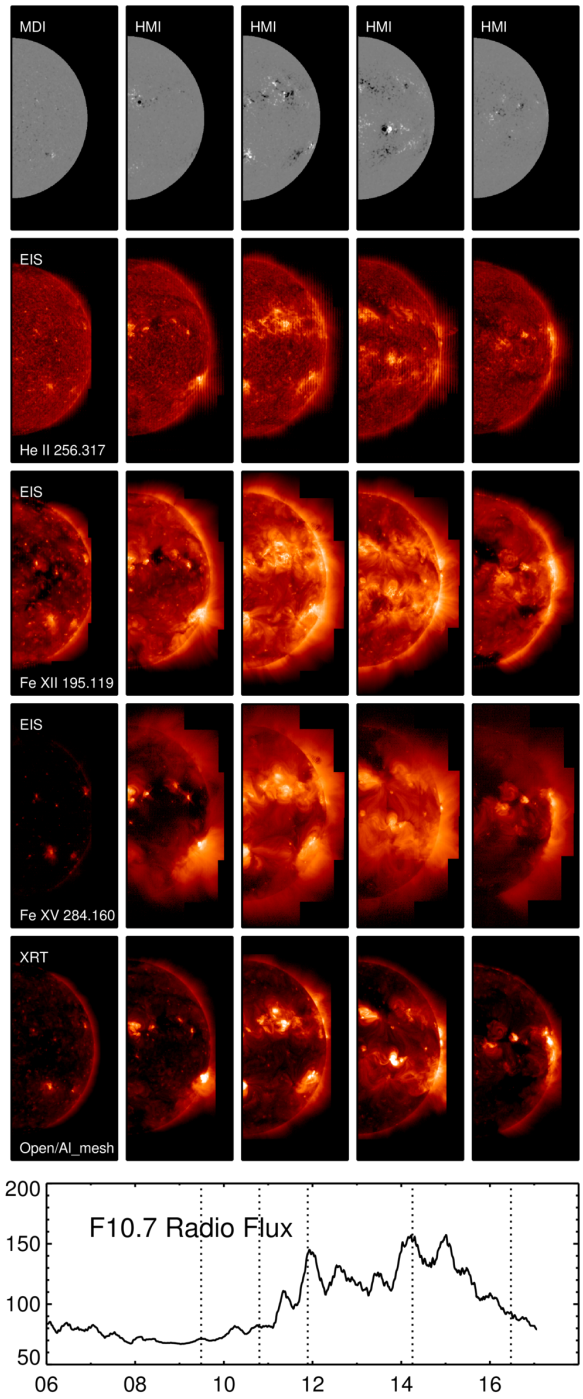

Figure 15: Selected full-disk synoptic images from MDI and HMI (top panels), EIS (middle panels), and XRT (bottom panels). The plot shows the evolution of the 81-day running mean of the F10.7 cm radio flux, a proxy for solar activity, during the Hinode mission.

Closely tied to irradiance observations are studies relating solar variability to stellar evolution. For example, Saar & Judge (2016) used SOT data, in part, to successfully measure plage areas on Sun-like stars by confirming that the depth of the SOT CN band closely follows the area of strong magnetic fields on the Sun.

Testa et al. (2015) also reviewed recent results in coronal activity and heating in cool stars – one of the focus areas being stars with very low, non-variable activity levels which may be in the stellar equivalent of solar magnetic grand minima (MGM). They identified a group of these potential MGM stars, and find that their coronae are very cool ($\sim$1 MK), and have flux levels similar to CHs. The group attempted to model the coronae of the nearest MGM candidate, τ Ceti, using solar coronal differential emission measures (DEMs) (Saar & Testa, 2012). The attempt was complicated by the fact that τ Ceti is very metal poor and lower mass than the Sun, and thus the solar DEMs could not be used unmodified. Indeed, direct application of solar CH DEMs failed to model the τ Ceti corona without unreasonable FIP effect adjustment.

Finally, Loftus et al. (2017) utilized the XRT flare catalog to explore the effect of nearby emerging flux (EF) on flare properties. The study found that EF-associated flares are 2x more likely to have associated eruptions, and those outside of ARs are on average stronger than those not connected to EFs. EF rates can thus be used as a proxy for heightened stellar activity.

Forward Work

The *Hinode* XRT and EIS instruments have now accumulated nearly a full solar cycle of full-disk irradiance observations. Further, these observations are unique in that they span the full range of solar plasma conditions, extending from the chromosphere to the hottest AR plasmas. The only comparable set of measurements was obtained by the Solar and Heliospheric Observatory's Coronal Diagnostics Spectrometer (*SoHO*/CDS) (Andretta & Del Zanna, 2014). These data, however, lacked coverage of the higher temperatures and are no longer being taken. Finally, unlike typical irradiance instruments, EIS and XRT have spatial resolution, which allows for detailed comparisons with the magnitude and structure of the underlying magnetic field. Thus, we now have a unique opportunity to study the magnetic origins of solar irradiance variability.

During this phase of the extended mission, *Hinode* will continue to observe, process, analyze, and distribute full-disk synoptic images that can be used for irradiance studies. XRT will continue to take daily full-disk images and EIS will continue to execute HOP 130 mosaics at a cadence of about once every three weeks. Further, we will extend the processing of these data to include a co-registered magnetogram from HMI or MDI (for dates before the launch of *SDO*) for each *Hinode* image. These combined data sets will definitively answer questions related to the solar cycle variability of the irradiance in different temperature and extreme ultraviolet (EUV) and SXR wavelength ranges. By comparing observations at various solar minimum and in the QS, it will be possible to quantify and compare irradiance variations at very low levels of activity. The density of the earth's thermosphere during the last solar minimum (2007–2009) was unusually low relative to historical measurements (e.g., Emmert et al., 2010; Solomon et al., 2010), but it is not clear if this is due to differences in the solar EUV irradiance or changing levels of geomagnetic activity during the past deep solar minimum.

2.4.2 Solar Cycle Evolution & Stability

The magnetic fields in solar polar regions are thought to be a direct manifestation of the global poloidal fields in the interior, which serve as seed fields for the global dynamo. Measuring magnetic field vectors in polar regions to reveal their spatial distribution from the ground is complicated by variable seeing from earth's atmosphere and a strong intensity gradient and foreshortening effect at the limb. The *Hinode*/SOT-SP polar observations are a breakthrough, and present a brand-new vision of polar magnetic fields.

The magnetic fields in polar regions are constructed from two magnetic components. One is a small magnetic patch with magnetic flux less than $\sim 10^{18}$ Mx. The net polarity of the patches located in a polar region is balanced, and there is no time dependence during a solar cycle. Therefore, it is argued that the patches are generated by local dynamo. The other component is a large magnetic patch with magnetic flux above $\sim 10^{18}$ Mx and located at boundaries of supergranulation cells in QS. The polarity and total magnetic flux of the patches is strongly dependent on the phase of a solar cycle and is a main contributor of global solar poloidal fields (Tsuneta et al. (2008), Ito

et al. (2010), Shiota et al. (2012)). Thus, the polarity inversion of solar poloidal fields is the time variation of the large magnetic patches in polar regions.

To investigate the polarity inversion in a solar cycle using polar fields, the *Hinode* mission has carried out polar monitoring observations every month since 2008, as one of its core programs. Figure 16 shows part of the program's observing sequence – blue & orange indicate the large magnetic patches. The time variation of the large magnetic patches clearly progresses with the polarity inversion at each polar region in Cycle 24. In the north, the decaying of the large magnetic patches with the previous cycle's polarity started in 2009. Most of them disappeared in 2013, but the patches with the new cycle's polarity did not appear in 2014 and 2015, during which the net magnetic field in the north was nearly zero.

The inversion process in the south polar region, however, was delayed, not beginning until the middle of 2013. In the map from 2016 (lower-left panel), we can finally begin to see the significant increase of the large patches. Because the process progressed rapidly and the distribution of magnetic fields in 2016 is similar to that at the previous solar minimum (except the polarity of the magnetic fields), Shiota & Shimojo (2017, in prep) surmise that the polarity inversion of the south polar region has already completed.

Hinode observations show that the north-south symmetry of the solar magnetic fields remains broken. Since the asymmetry of global magnetic fields appeared at Maunder minimum (Sokoloff & Nesme-Ribes, 1994), monitoring of polar regions is essential for predicting future activity. Will the asymmetry continue to next cycle, or will the evolution of magnetic fields in the northern hemisphere balance the polarity? To answer these questions, we need to continue polar monitoring observations with SOT-SP.

Petrie (2017) has made an independent analysis of the SOT-SP polar magnetic field observations from 2007 to 2016. First, a more careful analysis of the orientation of the vector fields and resolution of the 180 degree ambiguity was performed. Results showed that the strong magnetic concentrations (responsible for the net polarity) are approximately evenly-spread across the high latitudes, with no concentration or even a broad peak at the pole. This situation is different from the "top-knot" distributions that have been inferred from lower resolution LOS synoptics and that

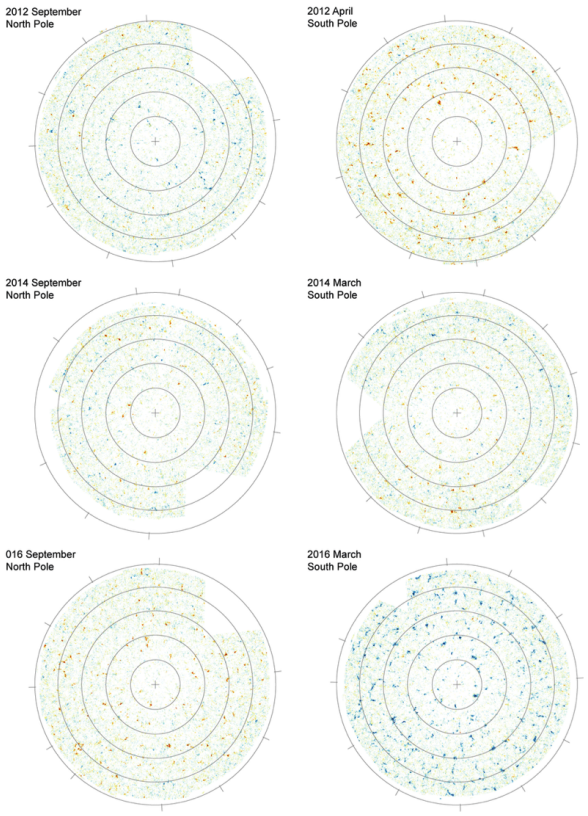

Figure 16: The landscapes of polar magnetic fields in 2012, 2014, and 2016. The center of each circle indicates north pole (left column) and south pole (right column). Blue (Positive) and Orange (Negative) show the polarity of the magnetic fields (Shiota & Shimojo 2017, in prep).

usually result from flux transport models including meridional flow. Petrie is reluctant to accept this result as definitive, however, citing the extreme foreshortening and hence reduced accuracy of the measurements at the pole, even with *Hinode* resolution.

The relative contributions of the strong and weak flux concentrations were then examined, finding results consistent with Shiota et al. (2012). The complex, latitude-dependent polarity reversals are shown clearly by the SP results. Petrie merged these with the National Solar Observatory's (*NSO*) Synoptic Optical Long-term Investigations of the Sun (SOLIS) results to make hybrid Carrington maps and PFSS field extrapolations into the heliosphere. Including SP maps leads to weaker and spatially more complex polar fields, since there is no top-knot distribution, with subtle changes in the heliospheric field patterns. A

similar merger of HMI and SP maps for the last 5 years would make an interesting comparison. Future *DKIST* polar field observations may solve the top-knot question, and comparison of those with simultaneous SP maps would greatly increase our confidence in both sets of polar measurements.

A significant finding reported in the previous Senior Review proposal was the lack of any solar cycle dependence of the weak IN fields, suggesting that they are caused by local dynamo action near the surface. Two groups have investigated this result further using different approaches. Jin & Wang (2015a,b) studied more than 1000 SP maps from 2008 to 2015 and confirmed no cycle variation, "exclud[ing] the possibility that the IN magnetic field mainly arises from the magnetic flux of decaying active regions." They also found that the IN flux density is independent of nearby ARs or enhanced network, strengthening the case for local dynamo origin. Faurobert & Ricort (2015) examined Fourier spectra of 98 QS SP maps from 2007 and 2013. They found only minor differences in spectra of IN regions but more in spectra of larger QS areas, which they ascribed to cycle differences in strong network fields. Utz et al. (2016) also looked at network fields using magnetic points in SOT synoptic G-band images as proxies. They found a component of those that follow the sunspot cycle with a time delay, presumably due to decay and dispersal of AR fields.

Forward Work

The *Hinode* synoptic programs have been observing the Sun with unparalleled uniformity since 2008, and in the next few years we will complete a solar cycle. Every three weeks, EIS makes a full disk spectral raster (HOP 130). Every month, all three instruments make a central meridian scan (HOP 79) and observe both polar regions (HOP 81). Every March and September when one pole is in view, SP maps every 3 days for a full rotation contribute to a mosaic of the vector magnetic field of the entire polar region (HOP 206). Many scientific results from these programs have been discussed in this Chapter and previous Senior Review proposals, and continuing them into the rising phase of a second solar cycle is one of our highest priorities. Some new observations that we plan to take are a full-resolution, large-area central meridian scan (possibly a partial synoptic map), to assist in calibration of HMI QS magnetic measurements, and coordinated polar field measurements with *DKIST* to cross-calibrate both instruments.

2.5 HSO Compatibility

The *Hinode* mission plays a significant role within the HSO and the greater NASA and ground-based observational infrastructure. Primarily through the HOP program, *Hinode* has provided complementary data sets used for a myriad of heliophysics research projects with 59 other missions and projects, involving at least 69 different instruments. Due to the fundamentally related science goals and capabilities, coordination with *IRIS* has become completely integrated into *Hinode* operation planning activities, to the point of combining the observational proposal structure into the *IRIS-Hinode* Operation Plan (IHOP) program. In fact, $\sim$80% of the proposals received since July 2013 have requested *IRIS* support. *NuSTAR* solar operations and coordination with XRT are maturing and are expected to provide critical constraints on high temperature plasma as solar conditions and Target of Opportunity campaigns become available for such observations. The first science run following on the heels of successful engineering runs with *ALMA* has recently been completed in January 2017 with accepted plans for future runs and follow-on upgrades. *Hinode* will also be a complementary resource for upcoming missions, namely, Solar Probe Plus, Solar Orbiter, *DKIST*, and a number of sounding rocket experiments dependent on *Hinode* data for verification and context.

2.6 Achievability

Hinode science research has been funded primarily by NASA and international research proposal programs and supplemented at a low level through core team support by the extended mission budget. Successful progress toward achieving the mission PSGs can be maintained through this funding paradigm. The core team is tasked with keeping the heliophysics community informed of *Hinode* progress, updates, and availability through conferences, publications, and outreach and is expected to collaborate with partners, both domestic and international, to ensure maximal usage of the observatory.

Table 1: Prioritized Science Goals with selected recent results and forward work. The goals are mapped to the 2014 Heliophysics Roadmap Research Focus Areas (RFAs) and 2012 Decadal Survey Challenges (DSCs). Select programs that take advantage of Focused Mode periods and the telemetry redistribution are noted.

§	SELECT RECENT RESULTS	FORWARD WORK
§ 2.1: PSG1 – Study the sources and evolution of highly energetic dynamic events.		
Relevant RFA(s): H1, F1, F2 **Relevant DSC(s):** SH 2 & 3		
Large-Scale Eruptive Events		
2.1.1	Strong upflows indicating explosive evaporation at post-flare loop footpoints from electron beams	Pre-eruptive active region (AR) monitoring; Flux tube eruptions; Improved *NuSTAR* coordination for high temperature AR constraints
Small-Scale Eruptive Events		
2.1.2	Presence of minor very hot plasma components in non-flaring ARs (possibly from reconnection); Evidence for non-thermal electron beam heating	Small-scale brightening (microflare) observations with very high cadence XRT image sets combined with EBTEL modeling
Flux Transfer & Magnetic Reconnection		
2.1.3	Direct evidence for reconnection in coronal loops of a small eruption via plasma heating; Strong indications of multi-threaded loop structures via electron beam analysis; New EIS density diagnostic	Prevalence of coronal jet spires as probes of particle acceleration mechanism
Telemetry Redistribution Program(s): EIS & XRT AR limb monitoring; On-disk high resolution SP maps		
Focused Mode Program(s): Coronal Mass Ejection (CME) watch; AR tracking; Limb tracking		
Primary Synergies: *IRIS*, *NuSTAR*, *ALMA*, *VLA*, *EOVSA*, *SDO*, *RHESSI*, *STEREO*		
§ 2.2: PSG2 – Characterize cross-scale magnetic field topology and stability.		
Relevant RFA(s): H1, F2 **Relevant DSC(s):** SH 2 & 3		
Active Regions		
2.2.1	XRT constraints on data-driven non-linear force-free field models of the coronal magnetic field; AR helicity analysis using SOT-SP revealing lack of region-to-region correlation	Active contributions to data-driven MHD simulations of AR evolution; EIS plasma heating constraints
Small-Scale Magnetic Fields		
2.2.2	Orientation of weak internetwork (IN) fields (dominantly horizontal) and contribution to global magnetic flux (entire network flux replaced in 10 hours)	IRIS-Hinode joint campaigns designed to address difficulty of assessing chromospheric heating effects of weak IN fields in quiet Sun (QS) and plage
Telemetry Redistribution Program(s): High cadence XRT image sets; Full EIS rasters with increased line coverage; High resolution SP maps; High cadence SP imaging		
Focused Mode Program(s): AR evolution; CME watch		
Primary Synergies: *IRIS*, *ALMA*, *SST*, *SDO*, GONG, Data-driven modeling, *DKIST*		

Continued on next page

Table 1 – continued from previous page

§	SELECT RECENT RESULTS	FORWARD WORK

§ 2.3: PSG3 – Trace mass and energy flow from the photosphere to the corona.

Relevant RFA(s): H1, F5
Relevant DSC(s): SH 2 & 3

Solar Wind		
2.3.1	Slow solar wind source regions identified and compared to *in situ* mass loss; Fast solar wind source studies under development; Discovery of inverse first ionization potential (FIP) effect abundances near sunspots	Coronal solar abundance studies; Abundance studies in periodic density structures in the high corona
Chromospheric Heating		
2.3.2	Observations of spicule heating into the transition region (TR) from the chromosphere; Evidence for sub-coronal wave heating in the umbra through shocks	Coordinations with *ALMA* and *IRIS* to connect the photospheric boundary with the dynamic chromosphere; Plage and AR monitoring to monitor emergence and weak field interaction
Magnetic Waves		
2.3.3	Indirect evidence of wave heating via resonant absorption and Kevlin-Helmholtz instabilties at loop boundaries; Wave property characterization using EIS non-thermal line width velocity	Combination of full vector field data with recently enhanced MHD wave models

Telemetry Redistribution Program(s): High cadence XRT image sets; Full EIS rasters with increased line coverage; High resolution SP maps; High cadence SP imaging

Focused Mode Program(s): AR evolution; EIS full-Sun scans

Primary Synergies: *IRIS*, *ALMA*, *ACE*, *SST*, *DST*, *STEREO*, *SDO*, *DKIST*

§ 2.4: PSG4 – Continue long term synoptic support to quantify cycle variability.

Relevant RFA(s): H1, F4
Relevant DSC(s): SH 1 & 3

Solar Irradiance		
2.4.1	Long baseline EIS & XRT synoptics monitor soft X-ray (SXR) irradiance since 2008; Stellar evolution studies based on solar variability	Continued long baseline campaign to monitor solar X-ray flux and EUV irradiance; Improve co-registration with HMI & MDI; Coordinated *IRIS*/EIS full disk mosaics
Solar Cycle		
2.4.2	Long baseline observations of polar field cycle variability; Asymmetric polar field reversal; Evidence for local dynamo origin of IN fields	Coordination between SP and *DKIST* to address polar field distribution; Continued long baseline campaigns to monitor magnetic field strength with the solar cycle

Telemetry Redistribution Program(s): Increased synoptics; SP scans

Focused Mode Program(s): Additional polar field mosaics

Primary Synergies: *IRIS*, *GOES*, *ACE*, *TIMED*, *SDO*, *SoHO*, *DKIST*, *NSO*/SOLIS

3 ACCESSIBILITY & IMPACT

3.1 Data Accessibility

Each PI-led team maintains a web accessible resident archive serving Level 0 data. The Solar Data Analysis Center hosted by GSFC maintains a replica archive of Level 0 data for each of the *Hinode* instruments. JAXA maintains the mission-wide Level 0, housekeeping, and raw data archives of all *Hinode* science, ephemeris, and spacecraft data. The Institute of Theoretical Astrophysics at the University of Oslo on behalf of the Norwegian Space Centre (NSC) and the European Space Agency (ESA) hosts the Hinode Science Data Centre Europe and provides an online resource for all science data products and tools for viewing QuickLook data products (available at http://sdc.uio.no/sdc/welcome). Refer to the Appendix for further information regarding access to calibrated data.

Uncalibrated, "QuickLook" data from the instruments are presented through web sites such as the Solar Monitor, Space Weather Browser at the Royal Observatory of Belgium, and the SolarSoft Latest Events service hosted by the Lockheed Martin Solar and Astrophysics Laboratory. The QuickLook data are available within hours of the observations. Additionally, an XRT synoptic database is maintained through Montana State University and is accessible via http://solar.physics.montana.edu/takeda/xrt_synoptics/latest_month.html.

Working with the *IRIS* team, we have developed a database for *Hinode* and *IRIS* observations, automatically populated with all data that overlap in space and time. The search tool http://www.lmsal.com/heksearch/ shows pointing, field of view, and measurement summaries for all instruments. When SOT or AIA datacubes coaligned with *IRIS* are available, links for downloading them appear in the results.

3.2 Research Access

All *Hinode* science data are available through the Virtual Solar Observatory (VSO; Hill et al., 2004) and the *Hinode* Science Data Center Europe. Online archives may be found via a number of channels:
http://hinode.msfc.nasa.gov/data_archive.html
http://sdac.virtualsolar.org/cgi/search
http://darts.isas.jaxa.jp/solar/hinode/query.php?A01=Go%20to%20Search
http://sdc.uio.no/search/API
http://helio.cfa.harvard.edu/XRT
http://www.lmsal.com/hek/hcr
http://solarb.mssl.ucl.ac.uk/SolarB/SearchArchive.jsp
http://sot.lmsal.com/data/sot/level1d
http://sot.lmsal.com/data/sot/level2d
http://www.csac.hao.ucar.edu

3.3 Community Use & Relevant Publications

The US instrument teams continue their scientific research at the low levels permitted by the extended mission budget. However, the vast majority of research with *Hinode* data is done by other domestic and international scientists and mission partners as well as by scientists in essentially every solar physics group around the world. The breakdown of recent publications by nation of origin (first author's institution), which is monitored in every Science Working Group (SWG) meeting, shows roughly proportional equal of publications by US, European, and Asian authors.

As of February 2017, *Hinode* science data have been used in at least 1095 refereed journal articles from scientists in more than 20 nations. The annual publications are shown in Figure 17. A searchable publication database maintained through NASA is available at: http://seal.nascom.nasa.gov/cgi-bin/bib_hui_seal.

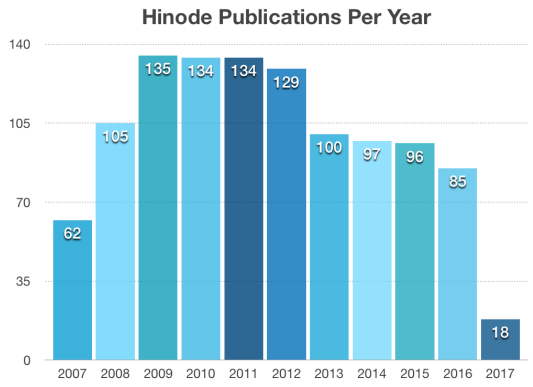

Figure 17: Hinode refereed publications per year.

A non-exhaustive survey of international universities and research institutes produced a list of at least 82 graduate students who have completed a Ph. D. thesis and 41 that have completed a Masters degree with *Hinode* data. A listing of the recorded theses can be found at: http://hinode.stelab.nagoya-u.ac.jp/en/publ/hinode_thesis.shtml/.

Since launch in 2006, ten *Hinode* science meetings have been held with the latest meeting in Nagoya, Japan attracting over 200 international scientists. Special sessions for *Hinode* observations and analysis have been held at AGU, AAS, IAU, COSPAR, AOGS, and IAGA meetings.

The use of HOPs to execute observing requests from scientists around the world represents another form of community use of *Hinode*. As of February 2017, there are 336 HOPs that have run or are planned to run in the near future. The *Hinode* science schedule coordinators plan the monthly observations and communicate this observation schedule to the instrument Chief Observers (COs) that create the weekly and daily science plans. Observation time is divided among core science team observation requests, synoptic observations, and external observations requests. Each HOP is listed at: http://www.isas.jaxa.jp/home/solar/hinode_op/hop_list.php. HOP productivity logs are maintained and updated regularly. Records of HOP productivity may be accessed at: http://hinode.msfc.nasa.gov/operations/hop_assessment/HOP_Productivity_Log.html.

TECHNICAL IMPLEMETATION

This section discusses the technical status of the mission and the mission extension proposed budget. Significant effort is continually directed toward ensuring efficient and responsive operations. Focused Mode operations were introduced just prior to the 2015 Senior Review and have since been successfully incorporated into the annual schedule during *Hinode* and *IRIS* eclipse periods. Also, telemetry allocation agility has greatly increased following the loss of the SOT-FG camera. This increased efficiency is fully consistent with the mission extension paradigm described in the Call for Proposals.

4 HINODE PROJECT OVERVIEW

Hinode is truly an international observatory, as scientists and engineers from all over the world come together through coordinated operations to produce ground-breaking solar observations. Figure 18 shows the international partners and other major participants in the *Hinode* mission. This high level organizational chart does not represent the extensive day-to-day interactions between the teams, which is presented later in the Hinode Project Organization Section (§ 4.2).

The *Hinode* observatory is comprised of three independently operated state-of-the-art instruments:

1. The Solar Optical Telescope (SOT) is a diffraction-limited, visible light telescope that provides the unparalleled combination of uninterrupted temporal coverage (free from atmospheric seeing, weather, and nighttime), high cadence (as short as 1.6 s), and 0.2″ spatial resolution over a significant 328″ × 164″ field-of-view (FOV). SOT is comprised of the Focal Plane Package (FPP), which is fed by the 0.5 meter Optical Telescope Assembly (OTA). The FPP consists of the Spectro-Polarimeter (SP) and (up to 2016) the Narrowband and Broadband Filter Imagers (NFI and BFI). The combined SOT system allows measurements of the vector magnetic field in the photosphere with unprecedented sensitivity (10 times better than previous instrumentation), while simultaneously observing the effects of these fields on the dynamics of both the photosphere and chromosphere.

2. The Extreme-ultraviolet Imaging Spectrometer (EIS) is an imaging spectrograph with very high spectral resolution which can detect Doppler flows and turbulent motions as small as 1-3 km s^{-1}, observing in two wavelength bands: 170-210 Å and 250-290 Å. EIS has high spatial resolution (1″ pixels), and has been the leader in providing detailed coronal temperature and density maps of active regions and transient phenomena such as flares over a wide temperature range (∼0.1 - 20 MK).

3. The X-Ray Telescope (XRT) has an unprecedented combination of X-ray spatial resolution (1″ pixels), full-Sun FOV (34′ × 34′), and image cadence capability (≤ 8 s) over a wide temperature range (< 1 to 30 MK). XRT has an extremely large dynamic range to detect the entire corona, from coronal holes to X-class flares.

Together these instruments combine to complete the outstanding science highlighted in § 2 and are

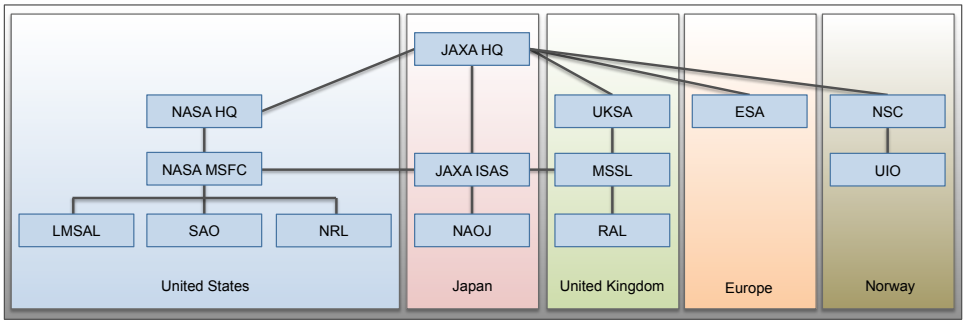

Figure 18: The Hinode International project organizational structure.

fully operational and capable of delivering the science planned with our PSGs from § 1.

4.1 Mission Operations

International teams on the ground operate the three *Hinode* instruments. The mission carries out its basic mandate to foster outstanding heliophysics research through planning meetings leading from scientific proposals, through coordinated observations, and ultimately to distribution of data to the community. The basic planning process is depicted in Figure 19.

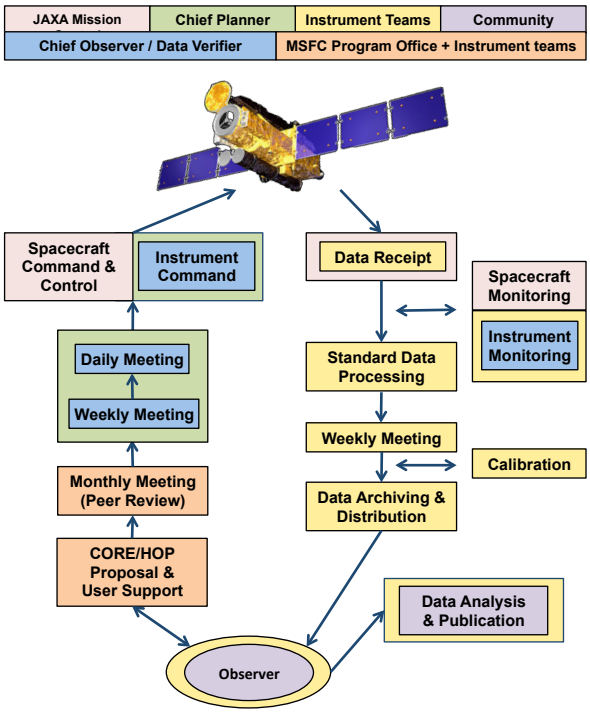

Figure 19: The end-to-end Hinode basic operations concept and data flow.

Each US PI team performs both operational and scientific functions; there is no centralized operations team. Each instrument team is comprised of international partners. The end result is a complex, though efficient, operational design which has worked well throughout the life of the mission.

Each instrument team's responsibilities include: 1) Assessing instrument health and performance; 2) Coordinating remotely with domestic and international partners, ground station controllers, and other scientists preparing *Hinode* observations; 3) Participating in planning activities (including Science Working Group activities) and coordinating campaigns with other missions or GBOs; 4) Analyzing calibration data and maintaining calibration software and documentation; 5) Performing science data analysis, investigations, and presenting scientific results through publications and presentations; 6) Ensuring instrument and scientific data and results are available to the research community and the general public.

With increasing experience, the efficiency of US *Hinode* operations has greatly increased in several key regards. The US instrument teams transitioned to remote operations following the Prime Phase wherein each team operates from a home institution instead of traveling to Japan. Science data are downlinked to the ground via S-band whereupon Levels 0 & 1 data are created automatically and made available for download via the VSO or other online databases.

During the extended mission, the Hinode Project Office (HPO) accepted higher operational risk and possible instrument degradation due to aging, which is fully consistent with the mission extension paradigm. As a consequence, the three US instrument teams have greatly reduced their level of engineering support; however, they continue to actively monitor and assess the instrument health and degra-

dation trends. The MSFC HPO does not maintain a contingency fund, fully funding the three instrument teams instead. If an anomaly occurs, support for the investigation comes from that team's regular funding.

4.2 Hinode Project Organization

Figure 20 depicts the organization of the HPO at MSFC. This office is responsible for managing and overseeing the three primary US instrument teams: LMSAL (SOT/FPP), NRL (EIS), and SAO (XRT). Several additional institutions continually participate in *Hinode* scientific operations beyond these three institutions, including: MSSL, NAOJ, Nagoya University, Kyoto University, MSFC, HAO, George Mason University, and Montana State University.

MSFC maintains overall budget and contract responsibility and provides limited technical and engineering support from the MSFC Engineering Directorate. Technical oversight covers systems engineering and other engineering support on an as-needed basis. The MSFC Project Scientist provides scientific oversight and reports instrument performance to the NASA Headquarters Program Scientist.

Instrument science operations are completed by Chief Observers (COs). COs are responsible for developing the science upload for the instrument and coordinating this plan with other instrument teams, the scientist requesting the observations, and instrument team leadership that is defining the observation schedule. The typical science upload requires a full workday to complete. US XRT and SOT currently handle half of all the annual CO duties for their instruments while the US EIS team handles one third.

The three instrument operations are coordinated by a Chief Planner (CP). CP duties include merging instrument commands to compile an integrated spacecraft load along with numerous scheduling activities.

4.3 Operations Cost Reductions

Through the prime mission phase and first mission extension, the role of CP was shared ~50/50 with Japan. From 2007 to June 2013, an MSFC Civil Service scientist filled this position for NASA with additional CP support from NRL. NRL continues to provide part time CP support in Japan for NASA following the return of the NASA civil servant to MSFC, which was done in order to reduce mission operations support costs. NASA CP duty support was thereby been reduced to 49 days (from ~78 days) as of October 2013.

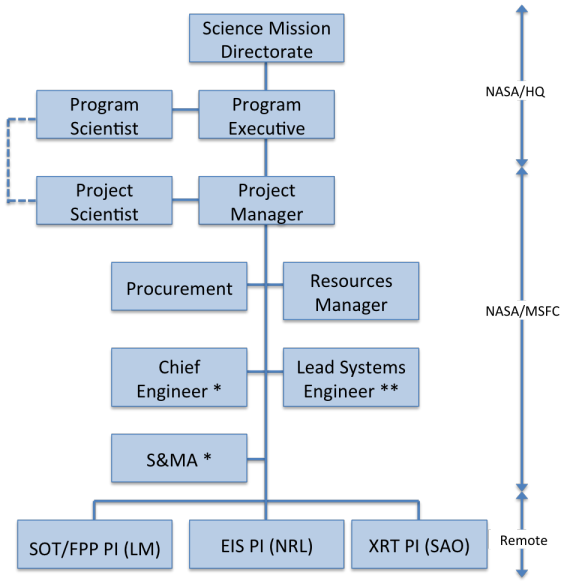

*Figure 20: HPO program management chart. *No cost to project. **As needed.*

Overall annual support for the NASA-sponsored instrument team operations was reduced by 15-20% following the 2013 Senior Review. So that the mission continues to operate safely and effectively on this significantly reduced budget, the HPO and instrument teams worked with international counterparts to develop operational strategies that reduce the net time required for operations planning while maintaining optimal periods of peak performance. The result of these efforts is *Focused Mode Operations*.

Focused Mode Operations

Hinode is an active observatory with inherently complex operations. Unlike observatories that observe an encompassing, continual FOV using a fixed observing program with ample bandwidth, *Hinode* is constrained to small observing areas, must adjust observing programs continually, and is limited by telemetry. However, these seemingly negative issues are precisely what allow *Hinode* to obtain cutting-edge resolution images with coordinated, efficient observing programs based on the target chosen by the community or core science team to achieve mission goals.

Solar conditions are continually changing, and as a predominantly activity-engaged mission, *Hinode* is

tasked to respond to them in order to maximize science outputs. This paradigm increases the cost of operations relative to automated observatories, which was duly anticipated during the development of Solar-B. While *Hinode* cannot be feasibly run as a fully automated observatory, the HPO has worked closely with the spacecraft and instrument teams to reduce operations with minimal impact on science.

Following two years of engineering tests and adjustments, Focused Mode Operations (the reduction of timeline creation from 3 times to once per week) have been executed safely twice annually since the 2015 Senior Review. While not a replacement for nominal operations, this new scheme has proven to be an effective method for streamlining *Hinode* operations while maintaining quality science output. The reduction of instrument operator duty accommodates the significant budget cuts from the 2013 Senior Review, **however, it does create a burden for international instrument teams not funded by NASA**.

Permanently operating under this schedule would not allow the mission to fully achieve its Prioritized Science Goals due to the inability to coordinate with *IRIS* and the inability to adequately respond to dynamic solar conditions, considering the FOVs and severe telemetry constraints involved. As such, Focused Mode Operations are scheduled only during the *Hinode* and *IRIS* eclipse seasons in order to reduce operations while maintaining maximal science output during periods of highly-anticipated operational activity. The schedule is also adjusted around peak *ALMA* coordination opportunities.

5 Spacecraft Status

Hinode is a Japanese mission insofar as the spacecraft, launch vehicle, and satellite-operations facility are provided by Japan. The *Hinode* spacecraft systems and operations are the responsibility of JAXA, and NASA does not typically participate in them.

The *Hinode* spacecraft was launched from the Uchinoura Space Center (Japan) on September 23, 2006 at 6:36 AM (JST) on a Japanese M-V launch vehicle into a circular, Sun-synchronous, polar low-Earth orbit (600 km altitude, 98.1° inclination). Upon verification that the spacecraft had successfully achieved orbit, the name was changed from Solar-B to *Hinode*. The prime mission began at the end of the initial engineering checkout period, so the official start of prime mission was on 2006 November 23. Thus, the *Hinode* Mission has completed its three-year prime mission and was granted mission extensions in 2010, 2013, and 2015. The spacecraft thruster system, which is primarily used for orbital control, has adequate fuel to continue the mission through well beyond a solar cycle.

The spacecraft functions are nominal and the attitude control system continues to provide good pointing stability performance. Data volume reached a new higher steady-state in the first mission extension through an increased number of station passes. The typical number of passes (8-12 minutes duration each) is currently 40-55 passes per day, including NASA contributions of 2-8 passes at Wallops and McMurdo and ESA contributions of 15 passes at Svalbard and Troll stations. This level of commitment is expected to continue for the foreseeable future. JAXA contributes an average of 30 S-Band ground station contacts daily. Data products are primarily acquired by careful consideration of FOV, pixel summing, selection of spectral lines, cadence, etc. in order to successfully mitigate performance reduction from the 2008 loss of the X-band telemetry system.

The *Hinode* spacecraft is in a polar orbit at about 680 km and thus has relatively high possibility for close approaches with debris and objects on orbit. The *Hinode* team has established the operational procedures for debris avoidance maneuvers (DAMs) and the JAXA flight dynamics facility continually monitors the potential for debris encounters with contributions and support from several US agencies. The *Hinode* spacecraft has executed a DAM in March 2012 for a very close approach of a small spacecraft. Sufficient station keeping and spacecraft maneuver fuel is available to continue observations for at least ten additional years in the current orbit.

6 Instrument Status

Minor problems have occurred since the prime phase with a significant technical issue for SOT described below; none of them were serious enough to jeopardize the scientific goals of the mission. Significant issues and mitigation strategies for each instrument are described below.

6.1 EIS

EIS has performed well since launch and the overall instrument status is nominal. The sensitivity of the instrument has been carefully monitored using QS observations and comparisons with EVE observations. The e-folding time for degradation is quite long: 6–7 years for the long wavelength channel and 9 years or longer for the short wavelength channel (see Del Zanna et al., 2013; Mariska, 2013; Warren et al., 2014, for details). The most recent calibration data suggests that the decay time for the long wavelength channel has slowed to match that of the short wavelength channel.

The EIS CCDs operate at a somewhat warmer than optimal temperature, which has lead to the formation of an increasing number of "warm pixels" on the detectors. These warm pixels are anomalously bright and cannot be used for analysis. By synthetically introducing warm pixels into data taken early in the mission, the impact of the warm pixels on the Gaussian fits to EIS spectral line profiles has been studied in detail and is documented in EIS Software Notes 6 and 13, which are distributed in SolarSoft. It was anticipated that when the warm pixels reached 30% of the detector area they would become problematic. In Febuary 2016 a three-day bakeout was undertaken and reduced the warm pixel count by 9%, to levels seen in 2012. Additional bakeouts are planned for the extended mission, which will improve instrument performance during solar minimum.

The seasonal pointing variations of EIS have been quantified through a regular alignment monitoring campaign and they are now incorporated in the timeline planning. One goal was to improve the EIS alignment with AIA, but it also greatly facilitates coordination with the *IRIS* instrument, enabling the instruments to be aligned to within a few arcseconds.

6.2 SOT / FPP

The significant change in SOT status is, of course, the loss of the FG camera. On February 25, 2016, the SOT CCD cameras (FG, SP, and CT) stopped functioning normally. This situation was quickly diagnosed as an electrical short circuit in the FG camera electronics, which overloaded the shared power converter, knocking out all 3 cameras. After the FG camera was shut off, the other two resumed operation with the same signal to noise ratios (SNRs) as before. Observing with the CT and SP has continued nominally since then. LMSAL engineers conducted a very detailed failure analysis, concluding that the short occurred in a capacitor in a noise filter in the FG analog electronics. At first, there was some hope that the FG camera could be repaired, based on the successful recovery of a similar camera fault on a previous mission. However, lab tests with a spare power converter showed that attempting to restart the FG camera would pose a risk of damage to the relay used to switch it on and off, with the possibility that it would be stuck on, thereby killing all 3 cameras. After peer review by other LM engineers, LMSAL recommended to NASA and JAXA that the FG camera remain off and observing continue with the SP; that recommendation was accepted by the *Hinode* projects and the SWG.

The other elements of SOT, the Optical Telescope Assembly, SP, and CT are all nominal. OTA focus and throughput to the two focal planes have been stable for several years, and light levels are now 70-80% of early mission values; there is no effect on performance except the sqrt(N) reduction in SNR, which can be compensated when desired by increasing SP integration times. The image stabilization system, polarization modulator, other electronics, and software continue to meet all requirements with no issues.

Responding to the FG loss and the ongoing importance of joint *IRIS* observations, the SOT team has continued to devise new observing programs to make repeated rasters with faster cadence, both in full spatial resolution (normal maps with 0.15" pixels) and in 2x2 summed resolution ("fast maps"). Following detailed magnetic evolution in the photosphere requires cadence of 2 minutes or less, permitting fields of view up to 6 to 15" wide in normal or fast map resolution, respectively. Of course, wider and slower rasters are possible, for example for sunspot structures or magnetic evolution in CHs or filament channels. The additional telemetry allows more normal maps to be taken, which enable PSF-compensated inversions of magnetic fields and atmospheric parameters. These produce the sharpest maps ever made along with some depth-dependence of physical properties, as in, for example, sunspots (Tiwari et al., 2015) or plage (Buehler et al., 2015). Additional time-series observations and

inversions of this type are planned for sunspot temporal evolution, polar fields, flux emergence, and cancellation in QS and AR explosive events, typically in coordination with *IRIS*.

Several improvements in SOT data processing have been made in the past year. Cross-correlation of all Ca H and G band images since late 2010 with AIA 1700 Å and HMI continuum images have produced accurate, absolute pointing coordinates, which are now included in Level 1 data product headers and correct other images (e.g., magnetograms) as well. The pointing errors in synoptic disk center and central meridian (HOP 79) images revealed a systematic *Hinode* pointing error, caused by a roll misalignment of the star trackers. The result has been LOS pointing errors up to 12" at the limb, which has caused *IRIS* and SOT rasters near the limb to be misaligned; this error will be corrected in future planning.

The *IRIS*, SOT, and AIA teams at LMSAL have been working with the University of Oslo (UiO) to make FG and AIA image datacubes that are aligned and remapped in space and time with *IRIS* datasets. These new cubes can be analyzed with the *IRIS* Solar SoftWare Interactive Data Language (SSWIDL) tools, `iris_xfiles` and `crispex`, as if they are additional *IRIS* slit jaw images. This access should make comparison of images with *IRIS* spectra much easier. The SP pipeline described by Lites & Ichimoto (2013) processes repeated raster time series as 2D maps, not xyt image cubes. New software is making cubes of Level 1 images and Level 2 inversion results, with time and pointing in headers and with missing columns detected and interpolated. These cubes can be read by the SSWIDL routines `read_sotsp` and `read_iris_l2`. Links on the *IRIS-Hinode* search pages for QuickLook movies and data distribution are in development, as well as remapped versions analogous to the FG and AIA cubes.

6.3 XRT

All science objectives are being achieved and the instrument is fully functional. Minor instrument difficulties exist but are being mitigated as follows:

Temperatures in the forward end of XRT have been higher than expected. A thorough analysis determined that these high temperatures are not a danger for the instrument due to sufficient thermal isolation of the mirror. The on-board limit tables for the temperatures were modified to reduce operational interruptions due to fluctuations in temperature close to the previous warning thresholds.

During the *Hinode* eclipse season, the rear of the XRT telescope becomes colder than during non-eclipse operations and filter wheel 1 (FW1) has experienced a weakened stepper encoder signal under these conditions. Consequently, in previous years the XRT team has elected to suspend use of FW1 during eclipse season in order to ensure continuous observations. However, due to the increase of the front end temperatures, the temperatures at the back of the telescope are now within safe ranges to operate FW1 during eclipse season. Since 2014, FW1 has been successfully operated during eclipse season with no issues. Operations of FW1 will continue as normal over the future eclipse seasons, maximizing science output from XRT at very little risk.

There is hydrocarbon contamination on the XRT detector and focal plane filters, which manifests in two ways. First, there is a time-dependent accumulation of a uniform layer over time. This accumulation is removed with a regular schedule of CCD bakeouts and monitoring. The effects on the data can be corrected with SSWIDL analysis software that applies a time-dependent contamination model adjusted with the monitoring data. Second, a constant residue of small spots have remained on the CCD since the initial bakeout, which is apparent when using the thinner filters. The spots on the images can be removed with routine processing software on the ground.

In May 2012 a sudden jump in intensity was observed in the G-band filter. The likely cause of this jump is a pinhole in one of the entrance filters. Calibration routines currently remove most of the visible light contamination from the X-ray images, and the development of more quantitative calibration routines are in the final stages of being completed. As a consequence, the C-poly and Ti-poly filters are no longer in use due to impact from the visible stray light; however, XRT was designed with filter redundancy. Al-mesh and Al-poly serve as viable substitutes for the retired filter set.

BUDGET

Hinode has been managed within budget since launch in 2006. The In-Guideline budget for FY17-FY23 is provided in Attachment I. Note the science return

from the NASA investment in *Hinode* enjoys very substantial leveraging from the mission support by the international partners (not included in this Review).

During the extended mission period, the project and instrument teams have placed a high priority on continually becoming more efficient in mission and data processing operations (§ 4.3), and the science research efforts of the instrument teams supported by the project are low. Any reductions below the inguidance budget would seriously impact the science observing and data availability. Lean, cost-effective operations are in place now, nearly eliminating any budgetary flexibility in the project.

Attachment I row descriptions are as follows:

1. FY17 22 NASA full-cost SMD guideline from September 2016 (PPBE18 Baselined Current Services MSFC by Project dated 02 September 2016). The budget provides for the continuation of the project through FY22, reflecting highly-efficient operations.

2. Total US mission budget for the HPO and all instrument teams. Cumulative values include lifetime Center Management & Operations (CM&O) beginning from the development phase and spans across NASA centers.

3. Labor, procurement, and travel budget for the HPO. FTE includes project & science management, operations management, and science analysis & support. WYE includes accounting functions, contractor support, science analysis, and operations support. Travel allotment supports conferences/workshops, SWG meetings, technical interchange meetings (TIMs), and reporting to HQs.

4.-6. Labor, procurement, and travel budget for each instrument team. WYE includes instrument & science management, operations management & support, systems engineering, administrative support, science analysis, and specialized engineering support. Travel supports conferences/workshops, SWG meetings, TIMs, and infrequent CO training trips to Japan. EIS funding also includes the CP support (§ 4.2).

7. Total Uncosted includes the contingency funds budgeted to ensure the instrument teams remain operational during the fiscal year transition. The Weeks of Uncosted is an estimate of the average number of work weeks that can be fully funded (based on the projected burn rate) using the expected amount of carry-forward funding. Prior experience indicates that ∼2 months of available funding is necessary.

8. In-kind costs for the communication passes provided by Wallops and McMurdo Stations. The Project Service Level Agreement (PSLA) defines the daily support of *Hinode* from the Wallops and McMurdo Stations as up to 8 passes a day. *Hinode* averages ∼7 passes per day. The cost of each pass is $508 and the average is for 365 days a year. An inflation rate is not added to the in-kind GSFC-provided costs.

Budget Summary

The HPO understands that the funding for the extended mission requires very high efficiency of operations and painful cuts in project-supported research. As the funding becomes efficiency-driven, more technical and scientific risk is assumed in the later years for the project as a whole and for each instrument. The extension includes mission operations and data analysis to ensure high quality science return. *Hinode* is currently observing the declining phase of the activity cycle, during which the largest flares are expected from large active regions, and will coordinate closely with *IRIS* and other new assets of the HSO. The *Hinode* team is convinced that we have made a compelling case for this extension and welcome the opportunity to discuss our mission with the panel.

BIBLIOGRAPHY

Allred, J. C., et al. 2015, ApJ, 809, 104

Andretta, V., et al. 2014, A&A, 563, A26

Antolin, P., et al. 2015, ApJ, 809, 72

Asgari-Targhi, M., et al. 2014, ApJ, 786, 28

Aulanier, G., et al. 2012, A&A, 543, A110

Barnes, W. T., et al. 2016a, ApJ, 829, 31

Barnes, W. T., et al. 2016b, ApJ, 829, 31

Barnes, W. T., et al. 2016c, ApJ, 833, 217

Brady, C. S., et al. 2016, ApJ, 829, 80

Brooks, D. H., et al. 2011, ApJL, 727, L13

Brooks, D. H., et al. 2015, Nature Com., 5947

Buehler, D., et al. 2015, A&A, 576, A27

Cargill, P. J., et al. 2012a, ApJ, 752, 161

Cargill, P. J., et al. 2012b, ApJ, 758, 5

Charbonneau, P. 1995, ApJS, 101, 309

Community SP Analysis Center. 2006, 10.5065/D6JH3J8D

de la Cruz Rodríguez, J., et al. 2016, ApJL, 830, L30

Del Zanna, G., et al. 2013, A&A, 555, 47

DeRosa, M. L., et al. 2015, ApJ, 811, 107
Doschek, G. A., et al. 2016, ApJ, 825, 36
Doschek, G. A., et al. 2015a, ApJL, 808, L7
Doschek, G. A., et al. 2015b, ApJL, 808, L7
Doschek, G. A., et al. 2016, ApJ, 832, 77
Dzifčáková, E., et al. 2016, A&A, 589, A68
Edwards, S. J., et al. 2016, Solar Physics, 291, 117
Emmert, J. T., et al. 2010, Geophys. Res. Lett., 37, L12102
Faurobert, M., et al. 2015, A&A, 582, A95
Fazakerley, A. N., et al. 2016, ApJ, 823, 145
Fujimura, D., et al. 2009, ApJ, 702, 1443
Gary, D. E., et al. 1997, ApJ, 477, 958
Gömöry, P., et al. 2016, A&A, 588, A6
Gošić, M., et al. 2016, ApJ, 820, 35
Guennou, C., et al. 2015, ApJ, 807, 145
Guglielmino, S. L., et al. 2016, ApJ, 819, 157
Hannah, I. G., et al. 2016, ApJL, 820, L14
Hara, H., et al. 2011, ApJ, 741, 107
Hara, H., et al. 2008, PASJ, 60, 275
Hill, F., et al. 2004, SPIE, 5493, 163
Hudson, H. S. 1991, Solar Physics, 133, 357
Imada, S., et al. 2015, Physics of Plasmas, 22, 101206
Ito, H., et al. 2010, ApJ, 719, 131
Janvier, M., et al. 2013, A&A, 555, A77
Janvier, M., et al. 2016, A&A, 591, A141
Jin, C., et al. 2015a, ApJ, 806, 174
Jin, C. L., et al. 2015b, ApJ, 807, 70
Kanoh, R., et al. 2016, ApJ, 831, 24
Klimchuk, J. A. 2015, PTRSL Series A, 373, 20140256
Klimchuk, J. A., et al. 2008, ApJ, 682, 1351
Kobelski, A., et al. 2016, in ASPC, Vol. 504, 327
Kobelski, A. R., et al. 2014a, Solar Physics, 289, 2781
Kobelski, A. R., et al. 2014, ApJ, 794, 119
Kobelski, A. R., et al. 2014, ApJ, 786, 82
Kobelski, A. R., et al. 2014b, Solar Physics, 289, 2781
Koch-Ocker, S., et al. 2016, ApJ, 832, 162
Kosugi, T., et al. 2007, Solar Physics, 243, 3
Laming, J. M. 2015, Living Reviews in Solar Physics, 12, 2
Landi, E., et al. 2010, ApJ, 711, 75
Landi, E., et al. 2014, ApJ, 787, 33
Lee, J.-Y., et al. 2015, ApJ, 798, 106
Lin, R. P., et al. 1984, ApJ, 283, 421
Lites, B. W., et al. 2013, Solar Physics, 283, 601
Lites, B. W., et al. 2017, ApJ, 835, 14
Loftus, K., et al. 2017, in AAS Abstracts, Vol. 229, 339.06
Loukitcheva, M., et al. 2015, A&A, 575, A15
Mariska, J. T. 2013, Solar Physics, 282, 629
Martínez González, M. J., et al. 2009, ApJ, 700, 1391
Matsui, Y., et al. 2012, ApJ, 759, 15
Moore, R. L., et al. 2010, ApJ, 720, 757
Murphy, N. A., et al. 2011, ApJ, 735, 5861
Narukage, N., et al. 2011, Solar Physics, 269, 169
Nindos, A., et al. 2015, ApJ, 808, 117
Ofman, L., et al. 1995, ApJ, 444, 471
Okamoto, T. J., et al. 2015, ApJ, 809, 71
Parker, E. N. 1988, ApJ, 330, 474
Petralia, A., et al. 2014, A&A, 564, A3
Petrie, G. 2017, Solar Physics, 292, 13
Reale, F., et al. 2009, ApJL, 704, L58
Reale, F., et al. 2009, ApJ, 698, 756
Reep, J. W., et al. 2016, ApJ, 827, 145
Reeves, K. K., et al. 2015, ApJ, 807, 7
Saar, S. H., et al. 2016, in 10.5281/zenodo.231291
Saar, S. H., et al. 2012, in IAU, Vol. 286, , 335
Savage, S. L., et al. 2010, ApJ, 722, 329
Savcheva, A., et al. 2016, ApJ, 817, 43
Savcheva, A., et al. 2015, ApJ, 810, 96
Savcheva, A. S., et al. 2012a, ApJ, 744, 78
Savcheva, A. S., et al. 2012b, ApJ, 759, 105
Schmelz, J. T., et al. 2016, ApJ, 833, 182
Schmelz, J. T., et al. 1996, ApJ, 473, 519
Seligman, D., et al. 2014, ApJ, 795, 113
Shearer, P., et al. 2014, ApJ, 789, 60
Shiota, D., et al. 2012, ApJ, 753, 157
Skogsrud, H., et al. 2015, ApJ, 806, 170
Sokoloff, D., et al. 1994, A&A, 288, 293
Solomon, S. C., et al. 2010, Geophys. Res. Lett., 37, L16103
Syntelis, P., et al. 2016, A&A, 588, A16
Takeda, A., et al. 2016, Solar Physics, 291, 317
Testa, P., et al. 2014, Science, 346, 315
Testa, P., et al. 2015, PTRSL Series A, 373, 20140259
Tian, H., et al. 2015, ApJ, 811, 139
Titov, V. S., et al. 2002, J. Geophys. Res., 107, 1164
Tiwari, S. K., et al. 2015, A&A, 583, A119
Tripathi, D., et al. 2011, ApJ, 740, 111
Tsuneta, S., et al. 2008, ApJ, 688, 1374
Utz, D., et al. 2016, A&A, 585, A39
van Ballegooijen, A. A. 2004, ApJ, 612, 519
Viall, N. M., et al. 2015, ApJ, 807, 176
Warren, H., et al. 2014, ApJS, 213, 11
Warren, H. P., et al. 2016, ApJ, 829, 35
Warren, H. P., et al. 2011, ApJ, 727, 58
Wedemeyer, S., et al. 2016, SSRv, 200, 1
Welsch, B. T. 2015, PASJ, 67, 18
Zhang, H., et al. 2016, ApJ, 819, 146

APPENDIX: MISSION ARCHIVE PLAN

Due to the international nature of the mission, the *Hinode* Science Center is located at the JAXA Institute of Space & Astronautical Science (ISAS) and serves as the primary archive for all *Hinode* data. Untransformed data and fully processed data, along with any higher level products, are archived and maintained as described in the following sections.

In addition, observatory products are documented in and linked from the Heliophysics Data Portal (HDP): http://heliophysicsdata.gsfc.nasa.gov). The *Hinode* portal can be directly accessed via: https://heliophysicsdata.sci.gsfc.nasa.gov/websearch/dispatcher?action=RESULT_LIST_PANE_ACTION&command=ProductViewCmd&resId=spase://VSPO/NumericalData/Hinode/PT1M.

The instrument teams include both veterans from before the launch and newer, younger members have recently joined to contribute to all aspects of the mission, thus ensuring continuity in operations, calibration, and data processing.

Mission Wide Data and Software

All science data are stored in FITS format. Analysis software is provided by each instrument team through SolarSoft. For each instrument a set of data products is available and are described by instrument in the following text. The primary source of ancillary data products for the *Hinode* mission is the SIRIUS Database maintained as part of the Mission Operations Center at ISAS. These data, which include all operational and engineering data and reports shared between the operations and instrument teams, are made available online except for the telemetry dictionaries, which are archived separately for security reasons. The DSN Schedule reports are archived and available on-line also.

Ephemerides and Attitude History: All *Hinode* ephemerides and attitude history files are provided as ASCII transfer format.

Telemetry: Final Level 0 telemetry files are archived by the resident archives for each of the instrument teams as well as the Solar Data Analysis Center at GSFC. Each resident archive also has a copy of all instrument housekeeping data. Japanese spacecraft data are not archived by NASA-supported institutions. After mission completion the final Level 0 data set will be maintained by SDAC.

SolarSoft: Data analysis software is distributed as part of the Solar Software Library also known as SolarSoft. This multi-mission software library is used extensively within the solar physics community, and enables cross-mission data analysis. The primary emphasis is on Interactive Data Language (IDL) software, but source code for other languages is also distributed using the SolarSoft mechanism. Together with the large generic library supplied with SolarSoft, each instrument team provides software for analyzing their own data. Also provided are the most current calibration data and the software required to calibrate the *Hinode* instrument science data.

Mission Documentation: A special issue of Solar Physics was devoted to the *Hinode* mission. In that issue extensive descriptions of the spacecraft, instruments, and ground systems are provided. See Kosugi et al. (2007) for an overview of the *Hinode* mission.

Data Distribution: The *Hinode* Science Center resides within the Solar Data Analysis Center (SDAC) at the Goddard Space Flight Center. The SDAC is a multi-mission Resident Archive with extensive experience distributing data for a number of missions, including *SoHO*, *TRACE*, *RHESSI*, *STEREO*, and others, as well as archiving data for older missions such as the Solar Maximum Mission. The SDAC will act as the active Resident Archive for the lifetime of the mission and beyond. Ultimately, the data will be delivered to the National Space Science Data Center (NSSDC) which will serve as the Permanent Archive. The Virtual Solar Observatory (VSO), http://www.virtualsolar.org, acts as the primary access point for all *Hinode* data, with the SDAC or the PI institution as the data provider. This maximizes the use of existing resources without duplication, and enables collaborative data analysis with other solar observatories. Data are also

available from the individual PI and Co-I institutions. A listing of all access sites is maintained at http://hinode.msfc.nasa.gov.

Higher-level, "semantic" descriptions of EIS, SOT, and XRT datasets are also available through the Heliophysics Event Knowledgebase (HEK, http://www.lmsal.com/hek) operated by LMSAL in conjunction with *SDO*. The HEK Coverage Registry (HCR) includes information on pointing, field-of view and instrument configurations (filters, wavelength cadence...) and are cross-referenced with solar events in the HEK Event Registry captured by data mining modules operating on incoming data from *SDO* and elsewhere. The HER and HCR are both searchable via the web-based http://www.lmsal.com/heksearch.

EIS MISSION ARCHIVE PLAN

Science Data Packets: EIS science observations are converted to Level 0 FITS files shortly after the telemetry files arrive at ISAS from the ground stations. Each data file contains one EIS "raster." For observations in which the EIS mirror scans the solar disk in slit or slot mode, the data in each spectral window can be used to construct a spectro-heliogram in the emission line or lines contained in the window. For observations in which the pointing remains fixed, the data in each spectral window can be used to construct the time history of each pixel along the slit or slot. Level 0 files can be examined using QuickLook software. EIS Level 0 FITS files can be converted to Level 1 FITS files using the SolarSoft IDL procedure EIS_PREP. This procedure removes detector bias and dark current, hot pixels, dusty pixels, and cosmic rays, and then applies a calibration based on the prelaunch absolute calibration. EIS_PREP also computes the statistical uncertainty for each spectral pixel and saves this information in an ancillary file. Both the Level 0 and Level 1 FITS files contain pointing and other information about the observation. The actual data are stored in a FITS binary table extension.

Documentation: Thumbnails of Level 0 data are available through the main EIS web page at MSSL (http://solarb.mssl.ucl.ac.uk/SolarB/). This web page serves as the central access point for EIS documentation, much of which is housed on the EIS WIKI. Additional documentation on instrument performance and software usage is provided in 21 EIS notes that are distributed in SolarSoft in the eis_notes subdirectory ($SSW/hinode/eis/doc/eis_notes).

Analysis Tools: EIS analysis tools are written in IDL and distributed through SolarSoft. Much of the software uses object-oriented programming, but non-object-oriented access tools are also provided.

Data Distribution: EIS Level 0 data are available through the Japanese DARTS system (http://darts.isas.jaxa.jp/solar/hinode/query.php?A01=Go%20to%20Search). Additional publicly available archives are accessible through the SDAC in the US, MSSL in the UK, and UIO in Norway. The MSSL and UIO archives are reachable through relational databases, which allow complex queries to be constructed. The SDAC archive is accessible through the VSO web-based interface, as well as through IDL software that accesses the VSO. Finally, information from the EIS as-run database has been incorporated into the LMSAL Heliophysics Event Knowledgebase (HEK) allowing for combined EIS-IRIS data searches (http://www.lmsal.com/heksearch/).

http://www.lmsal.com/heksearch/

SOT MISSION ARCHIVE PLAN

Science Data Products: All SOT image telemetry data are converted to FITS files upon receipt of the raw telemetry files at the ISAS Science Center from the ground stations. The FITS headers contain all information about the instrument parameters used to collect the image as well as the spacecraft pointing information. The images have been oriented to put the spacecraft north, which usually corresponds to solar north, at the top of the image, but no interpolations are done at this stage. The images can be converted to Level 1 by the user using a SolarSoft IDL procedure, FG_PREP or SP_PREP, which perform all of the calibration functions using the latest calibrations. Stokes spectra taken by the SP are calibrated and made available at Level 1 from both LMSAL and HAO, along with summary images of all SP rasters. Vector magnetic fields and other physical quantities inferred from Milne-Eddington inversions are made available at Level 2, along with error estimates.

Image (and spectra) header information is available in a database, accessible from the *Hinode* website at http://solar-b.nao.ac.jp/hsc_e/darts_e.shtml. Unified descriptions of SOT observing programs, including planning notes, timelines, browse images, and movies in PNG, JPEG and MPEG formats are available in the HCR.

Documentation: The following documentation and data products are also available via the SOT website: PNG browse images for most data, MPEG/Quicktime movies, image telemetry completeness data, instrument status, observation scheduling details, SOT Analysis Guide and tutorial (http://sot.lmsal.com/Data.html), SOT FITS Keyword Definition, and SOT Data Management Plan. A description of the instrument is given in Tsuneta et al. (2008). SOT operations and data documentation is also maintained by JAXA on-line at http://solar-b.nao.ac.jp/sot_e/.

Analysis Tools: SOT analysis tools are freely available through SolarSoft. SolarSoft is a set of integrated software libraries, data bases, and system utilities which provide a common programming and data analysis environment for Solar Physics. The following tools are currently available via SolarSoft: data browsers, data calibration, movie generation and display, image enhancement and visualization, polarized image processing, etc. "Panorama" and "browser," two high-performance image viewing tools, have also been developed and are available as part of the SolarSoft distribution. "Panorama" permits rapid review of FITS data using OpenGL graphics acceleration. Annotation software provides a means for registered users to record features and events found during these reviews into the Heliophysics Knowledgebase that has been developed for *SDO*. As these tools are improved and future tools developed, they will be added to the SolarSoft library. The SolarSoft library is maintained and distributed through NASA/GSFC solar physics program.

Final Data Archive: The SOT Level 0 data is final after the FITS files have been updated if any additional telemetry is received in the final (+30-day) raw telemetry stored in the SIRIUS database at ISAS. Currently, the NFI and BFI Level 1 (calibrated) products are the combination of the Level 0 FITS images and the FG_PREP IDL routine and calibration data files available in SolarSoft. This allows the user to take advantage of the evolving calibration of the instruments. The calibration files and parameters that are used in this package were revalidated in 2014 to ensure that they are up to date and able to generate Level 1 FITS files. Calibrations include corrections for instrumental artifacts such as flat field, dark offset, vignetting, and conversion to physical units. These final calibrations are currently being applied to all existing FG datasets to create final Level 1 FITS files ready for delivery to NASA. Level 0 data will be routinely used to generate Level 1 files for the foreseeable future. SP Level 1 and Level 2 data products are vetted by the scientists running the processing pipeline at HAO, so they are in final form when archived at LMSAL and HAO. The final archive will contain both the calibrated Level 1 files and the original Level 0 files for SP, NFI and BFI; and the Level 2 inversion results for SP.

Data Distribution: The primary site for storage of Level 0 FITS image data is the Japanese DARTS system. The primary means of querying data for analysis is by utilizing summary files which are read by SolarSoft tools. Data is freely available from LMSAL via web-based query at the LMSAL/SOT website. SPASE-compliant descriptions of SOT datasets are available through the Heliophysics Data Portal http://heliophysicsdata.sci.gsfc.nasa.gov. All of the data is synchronized daily to the NASA/GSFC SDAC directly from the DARTS site. SOT data are also available at the UIO archive in Norway. Visit http://www.lmsal.com/hek/hcr for a listing of recent events.

Virtual Observatory Access: The SOT SOC is serving SOT data through the Virtual Solar Observatory at GSFC/SDAC. The SOT team has worked with Dr. Joe Gurman at SDAC to implement full accessibility to the VSO community. VSO is committed to community interoperability efforts, such as the Space Physics Archive Search and Extract (SPASE) data model.

XRT MISSION ARCHIVE PLAN

Science Data Products: XRT science data are reformatted into Level 0 FITS files at ISAS/JAXA as receipt of all associated telemetry packages is confirmed. Level 0 files are 2-D FITS single-image files, which include a data array and a metadata section with a list of keywords. Level 0 data are converted into Level 1 data by the SolarSoft routine XRT_PREP, which subtracts a pedestal, removes high-frequency CCD read noise and and dark current noise, removes vignetting, and optionally normalizes for the exposure time and removes cosmic ray hits and streaks. The details of these calibrations can be found in Kobelski et al. (2014a). The Level 0 and the Level 1 FITS file metadata contain keywords that give information about the pointing and time of the observation, as well as other useful information about the observation.

XRT QuickLook data are produced in near real time by reformatting telemetry packages into Level 0 format FITS files as they arrive at IASA/JAXA. The QuickLook data are maintained as a separate database from the science data.

An official XRT Level 1 catalog is in place and served via the Virtual Solar Observatory. The data is processed with the latest version of XRT_PREP. Contiguous observations are aligned and de-jittered. Composite synoptic images are created out of long and short exposure pairs routinely collected during XRT synoptic observations.

XRT Data in Helioviewer: In addition to the standard FITS files available via the VSO, the data is available in JPEG2000 format for use with JHelioviewer. XRT images are currently incorporated into the Helioviewer web interface, and can be displayed and overlayed with images from other telescopes via https://www.helioviewer.org.

Co-alignment database: At the time of the last Senior Review, the XRT team had completed a multi-year project to improve calibration techniques and had begun to roll out a database of co-alignment coefficients so that every image from XRT could be effortlessly and accurately overlaid with images from SDO/AIA and HMI. The coalignment database is now completely automated: the data and the codes for correcting the image headers are distributed through SolarSoft, and the standard `xrt_prep` code includes the coalignment as one step in the preparation process, making it fully transparent to users. The database of coefficients is itself automatically updated weekly as new observations are placed in the archive. On average, the residual $[x, y, roll]$ errors after prepping the data are $[1.1'', 1.1'', 0.03^{\circ}]$ (3-σ level).

Documentation: QuickLook images of the twice-daily XRT synoptics are available on the web at the SAO/XRT website, as well as at daily monitoring sites such as Solar Monitor and the LMSAL Latest Events page. Documentation on the retrieval and processing of XRT data is given in the XRT Analysis Guide, as well as being provided as part of the XRT analysis software tree through SolarSoft. The analysis guide also includes information about the XRT FITS header keywords. Additionally, there are XRT science data tutorials available on the web.

Analysis Tools: XRT analysis tools are written in IDL and distributed publicly through SolarSoft. There are currently tools for data calibration, image processing, removing spacecraft jitter, calculating XRT effective area, calculating filter response as a function of temperature, calculating DEMs using XRT data, etc.

- http://xrt.cfa.harvard.edu/data/synoptics.php
- http://www.solarmonitor.org
- http://xrt.cfa.harvard.edu/resources/documents/XAG/XAG.pdf
- http://xrt.cfa.harvard.edu/science/tutorials.php
- http://www.lmsal.com/solarsoft/
- http://darts.isas.jaxa.jp/solar/hinode/query.php?A01=Go%20to%20Search
- http://sdac.virtualsolar.org/cgi-bin/search

ACRONYM LIST

”	arcsec
Å	Angstrom
ACE	Advanced Composition Explorer
AIA	Atmospheric Imaging Assembly (*SDO*)
AAS	American Astronomical Society
ALMA	Atacama Large Millimeter Array
Ar	Argon
B	Magnetic Field Strength
BFI	Broadband Filter Imager (SOT)
Ca	Calcium
CCD	Charged Coupled Device
CDS	Coronal Diagnostics Spectrometer
CH	Coronal Hole
CHIANTI	an atomic database for emission lines
CHROMIS	CHROMOspheric Imaging Spectrometer
CME	Coronal Mass Ejection
CM&O	Center Management & Operations
CN	Carbon Nitride
CO	Chief Observer
Co-I	Co-Investigator
CP	Chief Planner
CRISP	CRisp Imaging SpectroPolarimeter
CS	Civil Service
DAM	Debris Avoidance Maneuver
DARTS	Data ARchive and Transmission System
DEM	Differential Emission Measure
DKIST	Daniel K. Inouye Solar Telescope
DSC	Decadal Survey Challenge
DST	Dunn Solar Telescope
EBTEL	Enthalpy-Based Thermal Evolution of Loops
EIS	Extreme-ultraviolet Imaging Spectrometer
EOVSA	Expanded Owens Valley Solar Array
ESA	European Space Agency
EUV	Extreme-UltraViolet
EVE	Extreme Ultraviolet Variability Experiment (*SDO*)
Fe	Iron
FG	Filtergram (SOT)
FIP	First Ionization Potential
FOV	Field-of-View
FPP	Focal Plane Package (SOT)
FTE	Full Time Equivalent
FW	Filter Wheel
FWHM	Full Width Half Max
FY	Fiscal Year
G	Gauss
G-band	(visible light)
GOES	Geostationary Operational Environmental Satellite
GONG	Global Oscillation Network Group
GSFC	Goddard Space Flight Center
H-α	Hydrogen-alpha (line)
HAO	High Altitude Observatory
HDP	Heliophysics Data Portal
HMI	Helioseismic and Magnetic Imager (*SDO*)
HOP	Hinode Operation Plan
HQ	Headquarters
HPO	Hinode Project Office
HSO	Heliophysics System Observatory
HXR	Hard X-Ray
IBIS	Interferometric BIdimensional Spectropolarimeter
IDL	Interactive Data Language
IN	Internetwork
IRIS	Interface Region Imaging Spectrograph
JAXA	Japan Aerospace Exploration Agency
JST	Japan Standard Time
K	Kelvin
kG	kiloGauss
km	kilometer
LM(SAL)	Lockheed Martin (Solar and Astrophysics Lab)
LOS	Line-of-sight
LTE	Local Thermodynamic Equilibrium
m	meter
Mg	Magnesium

MHD	Magneto-hydrodynamic
MK	MegaKelvin
Mm	Megameter
MSFC	Marshall Space Flight Center
MSSL	Mullard Space Science Laboratory
Mx	Maxwell
NAOJ	National Astronomical Observatory of Japan
NASA	National Aeronautics and Space Administration
NFI	Narrowband Filter Imager (SOT)
NRC	National Research Council
NRL	Naval Research Laboratory
NSC	Norwegian Space Centre
NSO	National Solar Observatory
NuSTAR	Nuclear Spectroscopic Telescope Array
OTA	Optical Telescope Assembly
PI	Principal Investigator
PIL	Polarity Inversion Line
PM	Project Manager
PPBE	Planning, Programming, Budget and Execution
PSG	Prioritized Science Goal
PSLA	Project Service Level Agreement
QR	Quiet Region
QS	Quiet Sun
QSL	Quasi-Separatrix Layer
RFAs	Research Focus Areas
RHESSI	Reuven Ramaty High Energy Solar Spectroscopic Imager
ROSES	Research Opportunities in Space and Earth Sciences
s	second
S	Sulfur
Si	Silicon
SAO	Smithsonian Astrophysical Observatory
SDAC	Solar Data Center
SDO	Solar Dynamics Observatory
SECCHI	Sun Earth Connection Coronal and Heliospheric Investigation
SEE	Solar EUV Experiment
SMD	Science Mission Directorate
SoHO	SOlar and Heliospheric Observatory
SOLIS	Synoptic Optical Long-term Investigations of the Sun
SOT	Solar Optical Telescope
SP	Spectro-Polarimeter (SOT)
SSC	Science Scheduling Committee
SST	Swedish Solar Telescope
SSWIDL	SolarSoftware Interactive Data Language
STEREO	Solar TErrestrial RElations Observatory
SWG	Science Working Group
SXR	Soft X-Ray
SXT	Soft X-ray Telescope
T	Temperature
TIM	Technical Interchange Meeting
TIMED	Thermosphere Ionosphere Mesosphere Energetics and Dynamics
TRACE	Transition Region and Coronal Explorer
UAH	University of Alabama at Huntsville
UiO	University of Oslo
US	United States
UT	Universal Time
UV	Ultra-Violet
VLA	(Jansky) Very Large Array
VSO	Virtual Solar Observatory
WYE	Worker Year Equivalent
XRT	X-Ray Telescope